Eur. J. Mineral.
2002, **14**, 647-672

This paper was presented at the "Mica 2000"
meeting in Rome, Italy (November 2000)

Reactions and physical conditions during metamorphism of Liassic aluminous black shales and marls in central Switzerland

KENNETH J. T. LIVI[1,a)], JOHN M. FERRY[a)], DAVID R. VEBLEN[a)], MARTIN FREY[2,b)], JAMES A. D. CONNOLLY[c)]

[a)]The Morton K. Blaustein, Department of Earth and Planetary Sciences,
The Johns Hopkins University, Baltimore, Maryland 21218 USA
[b)]Institute of Mineralogy and Petrography, Bernoullistrasse 30, CH-4056 Basel, Switzerland
[c)]Institut für Mineralogie und Petrographie, ETH-Zentrum, Sonneggstrasse 5, CH-8082, Zürich, Switzerland

Abstract: The aluminous Liassic (lower Jurassic) shales, slates, and marls of the Central Swiss Alps were investigated by electron microprobe (EMP) and scanning electron microscopy (SEM) to determine the physical conditions of low grade metamorphism. The samples investigated experienced metamorphism from the diagenetic (100°C) to the epizonal grade (450°C). Temperatures estimated from Fe-Mg exchange equilibria between chlorite and chloritoid agree with calcite-dolomite geothermometry and previous workers' estimates. In the upper anchizone, calcite-dolomite temperatures record peak temperatures *ca*. 330°C. Epizone rocks in the Urseren Zone record *ca*. 400–450°C. Calculations of T–X phase equilibria in the CaO-MgO-FeO-Al_2O_3-SiO_2-H_2O-CO_2-CH_4 system with excess quartz and graphite were used to predict the stability fields of aluminous minerals and coexisting fluid compositions. The assemblage Sud + Dol + Qtz + Gr is stable over a temperature interval of 300–360°C. Calculations predict that, in CO_2-bearing fluids, reactions that form the index minerals margarite, sudoite, and chloritoid predominantly involve carbonate minerals. Margarite is not predicted to form in fluids dominated by CH_4. Temperatures recorded by T-X phase equilibria in the anchizone (330°C) agree well with calcite-dolomite thermometry. Temperatures recorded by T-X phase equilibria in the epizone (330–360°C) are significantly lower than calcite-dolomite temperatures (400–480°C).

The calculated fluid composition in the anchizone is CO_2-rich ($y_{CO_2} = CO_2/(CO_2 + H_2O) = 0.2$), whereas the epizone fluids are richer in H_2O ($y_{CO_2} = 0.02$–0.06). Fluid-flux calculations based on phase equilibria and reaction progress indicate that there was significant fluid infiltration in both the anchizone and epizone. The anchizone samples recorded a flux of *ca*. 6×10^3 cm^3 fluid/cm^2 rock with a flux increase to at least 2×10^5 cm^3/cm^2 in the epizone. These values are comparable to calculated fluxes during Devonian regional metamorphism in New England. Results show that careful mineral analysis can yield data appropriate for the estimation of sub-greenschist facies metamorphic conditions in aluminous low-grade rocks.

Key-words: Low-grade metamorphism, phase equilibria, aluminous shale, fluid infiltration.

Introduction

Very low-temperature metamorphism of shales and slates is traditionally studied by powder X-ray diffraction. Although this method is very useful for identifying the majority of the minerals present and measuring some indicators of relative metamorphic grade, textures and mineral compositions cannot be observed and measured directly. With the advent of improved electron microbeam instruments, such as electron microprobes (EMP) with good scanning electron microscopy (SEM) resolution, individual mineral grains can be imaged and analyzed. Microtextures and structures of shale minerals can be examined with the use of the transmission electron microscope (Peacor, 1992). Thus, fine-grained shales and slates can now be characterized almost as fully as their higher-grade counterparts. In doing so, researchers have revealed the heterogeneous nature of metaclastics, their tendency towards disequilibrium compositions and assemblages at the lower grades, and their numerous kinetic reactions (Merriman & Peacor, 1999; Livi *et al*., 1997). With this in mind, any application of equilibrium thermodynamics must consider the extent of equilibration, if any.

Assuming that equilibrium can be established, metamorphic conditions may be modeled through standard calculations of mineral equilibria, and mineral reactions responsible for the development of low-temperature index minerals in aluminous shales such as kaolinite, pyrophyllite, chloritoid, sudoite, and margarite can be determined. In addition, the formation of the index minerals can be related to conventional qualitative measures of grade such as illite "crystallinity". The goal of this study was to use electron microbeam instrumentation to determine metamorphic temperatures, fluid compositions, and fluid fluxes during low-grade metamorphism of aluminous clastic rocks from the Liassic in the Central Alps. Calculations of this sort have never been performed for such low-grade rocks.

---

[1]e-mail: klivi@jhu.edu; [2]Deceased

0935-1221/02/0014-0647 $ 11.70

DOI: 10.1127/0935-1221/2002/0014-0647

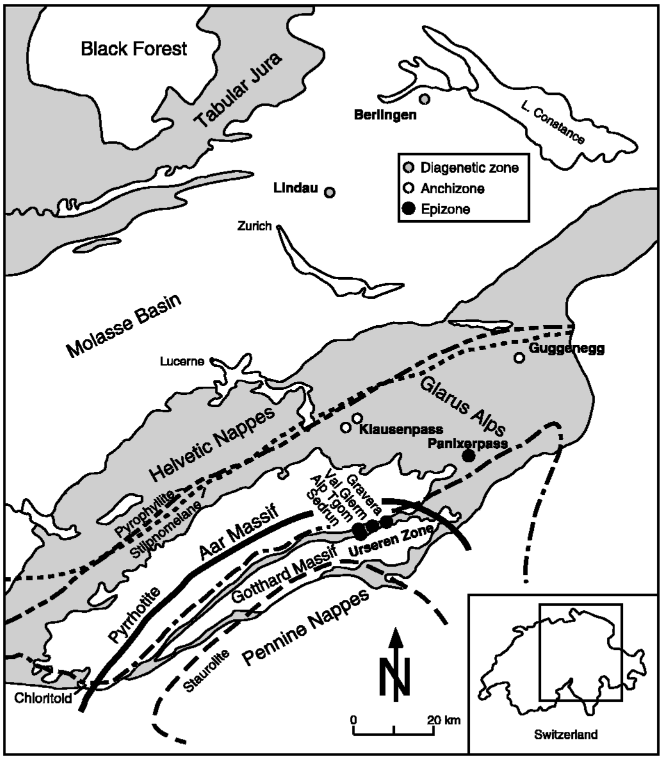

Fig. 1. Metamorphic map of the Central Swiss Alps showing sample locations. Modified from Frey (1978) and Rochette (1987).

It is to be expected that as the grade of metamorphism decreases, the occurrence of disequilibrium compositions will increase. Calculations involving elemental partitioning at low temperatures will most often be indicative of disequilibrium, and are not measures of the physical conditions of formation. This is reflected by large temperature range estimates and unreasonable temperature estimates. Although these data do not represent true metamorphic conditions, their convergence at higher temperatures measures progressive equilibration. Thus, an additional goal of this paper is to determine at what grade the Liassic shales have essentially equilibrated.

Geologic background

The Liassic (early Jurassic) clastic sediments can be found throughout central Switzerland (Fig. 1). The sediments were deposited in shallow marine environments (Trümpy, 1960), and metamorphism occurred during the Alpine orogeny (Frey, 1978). The clastic sediments are comprised of mudstones, shales, slates and marls and were sampled from the Jura mountains in the north, drill cores in the mollase basin, the Glarus Alps, and the Urseren Zone between the Aar and Gotthard massifs. The relative metamorphic grades were defined by illite "crystallinity" (IC) data (Kübler, 1967) obtained from associated paragonite-free Triassic Quartenschiefer samples because IC values for Liassic samples are complicated by the presence of Na-bearing micas.

Table 1. Minerals present.

Sample	B6	L6	L7	KP-2	MF-537	MF-551	MF-647	MF-650	OH-5	MF-736	MF-853
Location	Berlingen	Lindau	Lindau	Klausenpass	Klausenpass	Klausenpass	Guggenegg	Guggenegg	O. Hühnerkopf	Panixerpass	Alp Tgom
Grade	diagenetic	diagenetic	diagenetic	anchizone	anchizone	anchizone	anchizone	anchizone	anchizone	epizone	epizone
rock type	marl	shale	marl	sandstone	slate	slate	marl	slate	slate	marl	sandy slate
quartz	x	x	x	x	x	x	x	x	x	x	x
calcite	x	x	x			x	x	x		x	
dolomite	x	x	x	x	x	x	x	x		x	
pyrite	x	x	x		x	x	x	x	x	x	x
pyrrhotite											
anatase/rutile	x	x	x	x	x	x	x	x	x	x	x
K-feldspar	x	x	x								
albite	x	x	x					x			
kaolinite	x	x	x								
illite/smectite	x	x	x								
phengite/muscovite	x	x	x	x	x	x	x	x	x	x	x
paragonite					x	x	x	x			x
chlorite	x	x	x	x	x	x	x	x	x	x	x
sudoite				x			x		x		
donbassite							x		x		
pyrophyllite				x	x		x	x			
margarite											x
chloritoid											
tourmaline					x		x	x	x	x	
apatite	x	x	x			x	x	x		x	
REE-phosphate	x	x	x			x	x		x	x	x
allanite											x
zircon	x	x	x	x	x	x	x		x	x	x
gypsum	x										
barite	x										
organic matter	x	x	x	x	x	x	x	x	x	x	x

Analytical methods

Electron microprobe (EMP) analyses were performed at Johns Hopkins University with a JEOL 8600 Superprobe equipped with four wavelength-dispersive spectrometers (WDS) and a Tracor Northern (Noran) TN-5500 energy-dispersive spectrometer (EDS). Quantitative WDS analyses of chlorite and chloritoid laths ≥ 5 µm wide were obtained with a circular, 5 µm, defocused, 15-keV, 20 nA beam, with counting times of 60 seconds or until 0.5% precision was reached. Standards for silicates were albite for Na; enstatite for Mg; anorthite for Al, Si, and Ca; orthoclase for K; anatase for Ti; rhodonite for Mn; and fayalite for Fe. A 5 to 10 µm defocused beam was used for dolomite and a 10 to 20 µm beam for calcite. End-member carbonate minerals were used as standards for carbonate analyses. Data were reduced with the program CITZAF (Armstrong, 1989).

Doubly polished thin sections were mounted with Crystalbond and lightly coated with carbon. Backscattered electron (BSE) images were taken with the 8600 Superprobe at accelerating voltages between 15 and 30 kV. X-ray maps were generated with both EDS and WDS by rastering the beam over a stationary sample. In the case of the WDS, defocusing of the spectrometer was corrected by obtaining maps of standards under the same conditions as the unknown. The defocused standard intensity distribution (Ψ) of each spectrometer was smoothed by a median filter and normalized by Ψ_{max}/Ψ. When multiplied by the unknown map distribution, this refocuses the edges while leaving the focused center unaffected. X-ray maps of dimensions 128 × 128 pixels were collected simultaneously for the elements Na, Mg, Si, Al, K, Ca, and Fe. In addition, a region of interest in the EDS spectra spanned energies of the peaks for Zr, P, and S. The beam was held at 30 nA and 15 kV with a dwell time of 0.17 seconds. Each set of maps took approximately one hour to collect and between 25 and 40 areas (100 × 100 µm) were scanned per sample. The data were analyzed with the program MULTISPEC (Biehl & Landgrebe, 1993), which was designed for multiband remote sensing data. MULTISPEC characterizes the attributes of each mineral present by the intensity distribution of all eight maps within "training" fields. After being "taught" the intensities of all X-rays for each mineral, MULTISPEC classifies each pixel within the data, using a maximum-likelihood algorithm, and calculates modal abundances.

Mineralogy and petrography

The samples studied come from the Liassic black shales in central Switzerland (Fig. 1). Sample labels beginning with "MF" designate samples from the studies of Frey (1970 and 1978) that constitute a baseline to which results presented here may be compared. They were previously characterized carefully by X-ray powder diffraction (Frey, 1970 and 1978). Relative metamorphic grade is defined by illite "crystallinity" (Kübler, 1967) and ranges from the high diagenetic zone to the epizone. Samples from the three different zones include shale, marl, and sandstone. A list of minerals present is given in Table 1. General features

MF-855	MF-857	MF-886	MF-889	MF-897	MF-899	MF-900	MF-915	MF-920	MF-925	MF-928	MF-931	DrT 1210
Alp Tgom	Alp Tgom	Val Gierm	Val Gierm	Val Gierm	Val Gierm	Val Gierm	Gravera	Gravera	Gravera	Gravera	Gravera	Sedrun
epizone	epizone	epizone	epizone	epizone	epizone	epizone	epizone	epizone	epizone	epizone	epizone	epizone
sandy slate	sandy slate	slate	marl	slate	marly slate	marl	slate	slate	slate	slate	slate	marly slate
x	x	x	x	x	x	x	x	x	x	x	x	x
		x	x		x	x				x		x
		x	x		x	x				x		x
x	x	x	x	x	x		x	x	x	x	x	x
						x						
x	x	x	x	x	x	x	x	x	x	x	x	x
							?					
x	x	x	x	x	x	x	x	x	x	x	x	x
	x	x		x		x			x	x		
x	x	x	x	x	x	x	x	x		x	x	x
	x	x		x	x	x			x			
x	x			x	x		x	x	x	x	x	x
x	x		x			x		x	x	x	x	x
		x	x	x	x	x				x	x	x
x	x				x		x	x	x		x	
			x	x	x	x		x	x	x	x	x
x	x	x	x	x	x	x	x	x	x	x	x	x
				x								
x	x	x	x	x	x	x	x	x	x	x	x	x

Table 2a. Average diagenetic and anchizone-grade chlorite analyses.

Sample	B6	L6	L7	KP-2	KP-2	MF-537	MF-551	MF-647	MF-647	MF-647	MF650	OH-5	OH-5	OH-5
Phase *	Chl	Chl	Chl	Chl	Sud	Chl	Chl	Chl	Sud	Db	Chl	Chl	Sud	Db
Na_2O	0.29	0.09	0.07	0.09	0.25	0.02	0.01	0.04	0.09	0.05	0.01	0.03	0.09	0.10
MgO	13.05	11.60	8.97	4.89	3.23	6.78	8.83	10.18	9.97	2.00	7.55	6.10	4.93	1.17
Al_2O_3	21.70	21.92	23.28	25.06	37.94	23.70	23.36	24.53	35.40	44.56	23.92	25.33	27.07	43.32
SiO_2	36.91	30.08	27.60	25.63	37.44	26.66	25.31	23.77	34.72	36.35	26.71	25.17	28.21	38.33
K_2O	2.08	0.21	0.30	0.06	0.95	0.19	0.06	0.02	0.18	0.06	0.00	0.10	0.10	0.26
CaO	0.40	0.09	0.11	0.10	0.25	0.09	0.10	0.23	0.17	0.10	0.16	0.08	0.13	0.10
TiO_2	0.05	0.09	0.00	0.03	0.06	0.20	0.05	0.03	0.01	0.00	0.05	0.02	0.26	0.00
MnO	0.07	0.30	0.03	0.00	0.00	0.01	0.04	0.42	0.01	0.01	0.01	0.03	0.05	0.00
FeO †	10.41	25.23	27.28	32.40	8.93	30.92	30.86	29.18	5.44	1.51	30.31	31.33	27.41	3.77
Total	84.96	89.60	87.63	88.25	89.04	88.56	88.62	88.37	85.99	84.63	88.73	88.18	88.23	87.06
H_2O ‡	12.56	11.65	11.50	11.22	13.01	11.30	11.25	11.28	13.14	13.63	11.35	11.26	11.61	13.49
Total	97.52	101.26	99.13	99.47	102.04	99.86	99.87	99.65	99.13	98.26	100.07	99.44	99.84	100.55
Si	3.63	3.05	2.91	2.76	3.37	2.83	2.70	2.54	3.20	3.26	2.82	2.70	2.92	3.38
Al total	2.51	2.62	2.89	3.18	4.03	2.97	2.94	3.09	3.85	4.72	2.98	3.20	3.30	4.51
Al IV	0.37	0.95	1.09	1.24	0.63	1.17	1.30	1.46	0.80	0.74	1.18	1.30	1.08	0.62
Al VI	2.14	1.67	1.80	1.93	3.40	1.80	1.64	1.62	3.05	3.98	1.80	1.90	2.22	3.89
Ti	0.00	0.01	0.00	0.00	0.00	0.02	0.00	0.00	0.00	0.00	0.00	0.00	0.02	0.00
Fe^{2+}	0.86	2.14	2.40	2.91	0.67	2.75	2.76	2.60	0.42	0.11	2.68	2.81	2.37	0.28
Mg	1.91	1.75	1.41	0.78	0.43	1.07	1.41	1.62	1.37	0.27	1.19	0.97	0.76	0.15
Mn	0.01	0.03	0.00	0.00	0.00	0.00	0.00	0.04	0.00	0.00	0.00	0.00	0.00	0.00
Ca	0.04	0.01	0.01	0.01	0.02	0.01	0.01	0.03	0.02	0.01	0.02	0.01	0.01	0.01
Na	0.06	0.02	0.01	0.02	0.04	0.00	0.00	0.01	0.02	0.01	0.00	0.01	0.02	0.02
K	0.26	0.03	0.04	0.01	0.11	0.03	0.01	0.00	0.02	0.01	0.00	0.01	0.01	0.03
H	8.00	8.00	8.00	8.00	8.00	8.00	8.00	8.00	8.00	8.00	8.00	8.00	8.00	8.00
Total Cations	17.27	17.65	17.68	17.67	16.69	17.68	17.83	17.92	16.89	16.39	17.69	17.71	17.42	16.38
Total IV	4.00	4.00	4.00	4.00	4.00	4.00	4.00	4.00	4.00	4.00	4.00	4.00	4.00	4.00
Total VI	4.96	5.61	5.62	5.64	4.53	5.65	5.82	5.91	4.86	4.37	5.69	5.69	5.39	4.34
Total Inter	0.36	0.05	0.07	0.04	0.18	0.04	0.02	0.04	0.05	0.02	0.02	0.02	0.03	0.05
Fe# §	0.31	0.55	0.63	0.79	0.61	0.72	0.66	0.62	0.23	0.30	0.69	0.74	0.76	0.64

Note: * Chl = trioctahedral chlorite, Sud = di,trioctahedral chlorite, Db = dioctahedral donbassite; † All Fe as FeO; ‡ Assuming stoichiometric H; § Fe# = Fe/(Fe+Mg)

Table 2b. Average epizone-grade chlorite analyses.

Sample	MF-736	MF-853	MF-857	MF-886	MF-889	MF-897	MF-899	MF-900	MF-915	MF-920	MF-928	MF-931	DrT 1210
Phase*	Chl	Chl	Chl	Chl	Chl	Chl	Chl	Chl	Chl	Chl	Chl	Chl	Chl
Na_2O	0.08	0.06	0.05	0.07	0.08	0.02	0.01	0.00	0.04	0.01	0.04	0.02	0.02
MgO	13.57	11.22	13.82	13.36	14.01	13.87	8.51	6.51	9.42	16.07	14.92	13.43	10.83
Al_2O_3	25.46	24.41	24.70	24.95	24.78	24.48	25.22	23.99	23.80	25.42	25.91	25.27	24.72
SiO_2	26.27	24.78	24.97	25.91	25.41	25.14	24.18	23.85	25.86	27.62	25.28	25.98	24.22
K_2O	0.20	0.08	0.01	0.05	0.00	0.03	0.13	0.02	0.00	0.02	0.03	0.07	0.05
CaO	0.15	0.01	0.02	0.07	0.04	0.02	0.25	0.11	0.04	0.00	0.29	0.01	0.14
TiO_2	0.10	0.02	0.10	0.06	0.10	0.36	0.04	0.15	0.08	0.00	0.07	0.08	0.06
MnO	0.06	0.09	0.14	0.05	0.02	0.00	0.03	0.08	0.02	0.00	0.07	0.00	0.10
FeO †	22.28	27.54	24.75	23.96	24.06	23.72	30.52	34.13	29.24	18.79	21.00	23.23	28.95
Total	88.16	88.19	88.57	88.47	88.51	87.64	88.89	88.83	88.50	87.94	87.62	88.09	89.08
H_2O ‡	11.74	11.42	11.57	11.65	11.63	11.63	11.25	11.05	11.37	11.99	11.79	11.70	11.33
Total	99.90	99.61	100.13	100.11	100.13	99.27	100.14	99.88	99.87	99.94	99.41	99.80	100.41
Si	2.68	2.61	2.58	2.66	2.62	2.61	2.57	2.59	2.73	2.76	2.59	2.67	2.55
Al total	3.07	3.04	3.01	3.02	3.01	3.00	3.16	3.07	2.96	3.00	3.13	3.06	3.07
Al IV	1.32	1.39	1.42	1.34	1.38	1.39	1.43	1.41	1.27	1.24	1.41	1.33	1.45
Al VI	1.75	1.65	1.60	1.69	1.63	1.61	1.73	1.67	1.70	1.76	1.72	1.73	1.62
Ti	0.01	0.00	0.01	0.00	0.01	0.03	0.00	0.01	0.01	0.00	0.01	0.01	0.00
Fe^{2+}	1.90	2.43	2.14	2.06	2.07	2.06	2.72	3.10	2.58	1.57	1.80	2.00	2.55
Mg	2.07	1.76	2.13	2.05	2.15	2.15	1.35	1.05	1.48	2.40	2.28	2.06	1.70
Mn	0.01	0.01	0.01	0.00	0.00	0.00	0.00	0.01	0.00	0.00	0.01	0.00	0.01
Ca	0.02	0.00	0.00	0.01	0.00	0.00	0.03	0.01	0.00	0.00	0.03	0.00	0.02
Na	0.02	0.01	0.01	0.01	0.02	0.00	0.00	0.00	0.01	0.00	0.01	0.00	0.00
K	0.03	0.01	0.00	0.01	0.00	0.00	0.02	0.00	0.00	0.00	0.00	0.01	0.01
H	8.00	8.00	8.00	8.00	8.00	8.00	8.00	8.00	8.00	8.00	8.00	8.00	8.00
Total Cations	17.79	17.88	17.91	17.83	17.88	17.86	17.85	17.86	17.78	17.74	17.85	17.80	17.91
Total IV	4.00	4.00	4.00	4.00	4.00	4.00	4.00	4.00	4.00	4.00	4.00	4.00	4.00
Total VI	5.75	5.86	5.90	5.81	5.86	5.85	5.83	5.86	5.78	5.73	5.84	5.79	5.90
Total Inter	0.06	0.02	0.01	0.03	0.02	0.01	0.05	0.02	0.01	0.01	0.04	0.01	0.03
Fe# §	0.48	0.58	0.50	0.50	0.49	0.49	0.67	0.75	0.64	0.40	0.44	0.49	0.60

Note: * Chl = trioctahedral chlorite, Sud = di,trioctahedral chlorite, Db = dioctahedral donbassite; † All Fe as FeO; ‡ Assuming stoichiometric H; § Fe# = Fe/(Fe+Mg) of the samples are described below and addition data given in Livi *et al.* (1997).

Diagenetic zone

Marls contain quartz grains that show evidence of compaction and overgrowth before cementation by calcite and gypsum in some cases. The quartz grains show good rounding, are fractured (possibly in place), and have long grain-to-grain contacts. Calcite in the shales is distributed throughout the clay matrix as micrometer-sized grains or as shell fragments. In the marls, dolomite rhombs rimmed by ankerite have grown into pore space and are also found within the clays of both the marls and shales. In both rock types, pyrite is often found as octahedral inclusions in calcite and dolomite and as framboids. Albite and K-feldspar are detrital, and their irregular outlines and pitted appearances indicate they were dissolving. Kaolinite occurs in vermicular books, as massive collections of small grains within shells, and between quartz grains. Illite/smectite (I/S) is the dominant clay mineral and is concentrated in silty laminations in the marls. I/S sheets wrap around detrital minerals. Detrital muscovite occurs as long, thin laths that are often split or frayed at the ends. Kaolinite commonly partially replaces detrital muscovite. Occasional stubby but well-formed laths of phengite may be porphyroblasts. Chlorite laths occur in low concentrations, except in sample K7 from Kreuzlingen which contains abundant chlorite and berthierine with little I/S or kaolinite. Some chlorite crystals are obviously detrital, but many cannot be unequivocally identified as either detrital or authigenic. Glauconite occurs as spherical pellets and within the clay matrix of samples from Frick (see Livi *et al.*, 1997). Accessory minerals include apatite, monazite, xenotime, zircon, tourmaline, titanium oxide (either anatase or rutile), and organic matter.

Anchizone

Slates in the anchizone differ from diagenetic shales in three major ways: (1) increased evidence and intensity of compaction features, (2) different sheet silicate mineralogy, and (3) the formation of phyllosilicate "stacks" (Livi *et al.*, 1997). Quartz grains that are suspended in a phyllosilicate matrix have irregular, pitted outlines. In some samples, calcite has formed within the pressure shadows of larger quartz grains. When concentrated in layers or within sandstone, quartz grains have interlocking boundaries. Most features of the carbonate minerals are the same as in the diagenetic zone. Kaolinite is absent from the anchizone samples of this study, except for occasional layers that appear to be veins of retrograde alteration. Four new sheet silicates appear. Pyrophyllite occurs in about half of the samples. Paragonite, or its precursor brammallite (Livi *et al.*, 1997), is found in most samples. Detrital muscovite remains and is often intergrown with pyrophyllite. There is an increase in the abundance of smaller, well-formed phengitic muscovite grains in the phyllosilicate-rich regions. The aluminous chlorite minerals sudoite (di-trioctahedral) and donbassite (dioctahedral) appear either separately or together. They are most easily identified within phyllosilicate stacks. These stacks can contain any combination of mica and/or chlorite. Fe-rich chlorite occasionally forms spherical aggregates that may have cores of pyrophyllite. Many of the Fe-rich chlorite minerals are intergrown with berthierine.

Epizone

The major mineralogical changes in the transition from the anchizone to the epizone are the appearance of margarite and chloritoid, the disappearance of pyrophyllite, and the increased size and better-developed morphology of phyllosilicate grains. Margarite normally does not form large crystals but is intimately mixed with paragonite and muscovite (Livi *et al.*, 1997). Paragonite is concentrated along the boundaries of muscovite laths and does not often occur as discrete grains. Muscovite and chlorite penetrate calcite and quartz grains, compared to wrapping around detrital grains at lower grades. Phyllosilicate-rich "P" and quartz- and carbonate-rich "Q" domains are developed. The sheet silicates in the "Q" domains tend to form at high angles to the sheet silicates in the "P" domains. Chloritoid laths usually contain quartz inclusions and commonly crystallize in collections of rosettes that cut across the schistosity. Some samples contain dolomite that is pitted and partially dissolved.

Mineral compositions

Chlorite

Average chlorite analyses are given in Tables 2a and b. Chlorite grains in the diagenetic and anchizonal grade rock may be very fine-grained. Therefore, care was taken to avoid overlaps with other minerals especially white micas. Besides the more common trioctahedral chlorite, analyses for the sudoite and donbassite are included. The vacancy-rich species were identified mainly on the basis of electron microprobe analyses. In samples MF-647 and OH-5, all three species are found. In general, the octahedral vacancy content of the epizone chlorite averages are lower than those of lower grade.

Chloritoid

Average analyses are presented in Table 3. Chloritoid exhibits very little chemical variation. Chloritoid laths commonly contain abundant quartz inclusions, which may explain, in part, Si concentrations over 2 cations per formula unit. The inclusions may also be products of the chloritoid-forming reaction. Transmission electron microscope images show that chloritoid crystallizes without inclusions of sheet silicates but may have considerable stacking disorder, consistent with observations of Banfield *et al.* (1989).

Table 3. Average chloritoid analyses.

Sample	MF-853	MF-857	MF-897	MF-899	MF-915	MF-920	MF-925	MF-928	MF-931	DrT 1210
Na_2O	0,02	0,05	0,03	0,05	0,02	0,01	0,03	0,02	0,01	0,01
MgO	1,94	2,52	2,56	2,03	1,26	2,45	2,61	2,06	1,93	1,90
Al_2O_3	40,90	41,35	40,93	41,07	40,32	40,85	41,11	41,39	41,56	41,32
SiO_2	24,66	24,84	25,02	25,43	24,67	25,22	24,72	24,84	24,84	24,21
K_2O	0,06	0,01	0,03	0,34	0,00	0,00	0,04	0,03	0,05	0,01
CaO	0,00	0,03	0,02	0,19	0,01	0,01	0,02	0,12	0,01	0,05
TiO_2	0,06	0,06	0,15	0,44	0,00	0,05	0,29	0,22	0,30	0,31
MnO	0,26	0,32	0,04	0,09	0,32	0,20	0,31	0,24	0,07	0,24
FeO*	24,77	23,43	23,62	23,61	25,91	23,70	23,34	24,43	24,16	25,13
Total	92,66	92,61	92,40	93,25	92,51	92,49	92,47	93,34	92,93	93,17
H_2O †	7,28	7,33	7,33	7,32	7,24	7,33	7,33	7,30	7,32	7,26
Total	99,94	99,94	99,73	100,58	99,75	99,82	99,79	100,63	100,24	100,44
Si	2,032	2,034	2,052	2,070	2,049	2,067	2,028	2,027	2,031	1,989
Al total	3,973	3,990	3,957	3,939	3,947	3,947	3,974	3,981	4,004	4,001
Al^{IV}	1,968	1,966	1,948	1,930	1,951	1,933	1,972	1,973	1,969	2,011
Al^{VI}	2,006	2,023	2,009	2,009	1,996	2,014	2,002	2,008	2,035	1,990
Ti	0,003	0,004	0,009	0,027	0,000	0,003	0,018	0,014	0,018	0,019
Fe^{2+}	1,707	1,604	1,620	1,607	1,800	1,625	1,601	1,667	1,652	1,727
Mg	0,238	0,307	0,313	0,247	0,156	0,300	0,319	0,250	0,235	0,233
Mn	0,018	0,022	0,003	0,006	0,023	0,014	0,022	0,017	0,005	0,017
Ca	0,000	0,003	0,002	0,016	0,001	0,001	0,002	0,010	0,001	0,005
Na	0,003	0,007	0,004	0,007	0,003	0,001	0,004	0,003	0,002	0,002
K	0,007	0,001	0,003	0,035	0,000	0,000	0,004	0,003	0,005	0,001
H	4,000	4,000	4,000	4,000	4,000	4,000	4,000	4,000	4,000	4,000
Total Cations	11,983	11,972	11,964	11,955	11,979	11,957	11,972	11,972	11,953	11,993
Total IV	4,000	4,000	4,000	4,000	4,000	4,000	4,000	4,000	4,000	4,000
Total VI	3,972	3,963	3,956	3,912	3,976	3,956	3,963	3,966	3,945	3,990
Fe# ‡	0,878	0,839	0,838	0,867	0,920	0,844	0,834	0,870	0,876	0,881

Note: * = All Fe as FeO; † = Assuming stoichiometric H; ‡ = Fe/(Fe+Mg)

Table 4a. Average calcite analyses.

Sample	B6	L6	L7	MF-551	MF-647	MF-650	MF-736	MF-886	MF-889	MF-899	MF-900	MF-928	DrT 1210
MgO	0.54	0.64	0.55	0.59	0.65	1.37	1.03	1.21	1.69	1.20	0.79	0.25	1.01
CaO	53.47	54.46	54.22	53.27	54.56	53.14	53.32	52.25	49.07	50.92	51.90	53.87	53.21
MnO	0.26	0.15	0.14	0.19	0.11	0.29	0.05	0.21	0.15	0.47	0.22	0.24	0.21
FeO *	0.82	0.38	0.45	1.92	0.64	1.66	1.36	1.69	2.86	3.32	2.09	0.93	2.26
total:	55.08	55.63	55.35	55.97	55.96	56.46	55.77	55.36	53.76	55.91	55.00	55.29	56.69
CO_2†	43.96	44.03	44.01	43.87	44.01	44.02	44.01	44.00	43.97	43.81	43.88	43.90	43.91
Total	99.04	99.66	99.36	99.84	99.97	100.48	99.78	99.35	97.73	99.72	98.89	99.19	100.59
Fe^{2+}	0.012	0.005	0.006	0.027	0.009	0.023	0.019	0.024	0.042	0.047	0.030	0.013	0.031
Mg	0.014	0.016	0.014	0.015	0.016	0.034	0.026	0.030	0.044	0.030	0.020	0.006	0.025
Mn	0.004	0.002	0.002	0.003	0.002	0.004	0.001	0.003	0.002	0.007	0.003	0.003	0.003
Ca	0.971	0.977	0.978	0.956	0.973	0.939	0.954	0.943	0.913	0.917	0.947	0.977	0.941
Fe# ‡	0.463	0.250	0.314	0.647	0.358	0.404	0.425	0.438	0.488	0.609	0.597	0.679	0.557

Note: * = All Fe as FeO; † = assuming stoichiometric C; ‡ = Fe/(Fe+Mg)

Carbonate minerals

Average analyses are presented in Tables 4a and b. Dolomite grains are usually zoned with rounded cores of nearly pure $CaMg(CO_3)_2$ overgrown by euhedral, Fe-rich rims. The cores probably represent detrital dolomite grains. The rims grew sometime in the early to middle diagenetic zone, because the lowest-grade samples from northern Switzerland already contain ankerite rims (KLF4 and KLF2 from Frick, Livi *et al.*, 1997) with dolomite cores too small for EMP analysis.

Cation exchange equilibria

Chloritoid-chlorite

Laird (1988), Ghent *et al.* (1987), and Ashworth & Evirgen (1984) reviewed published Fe-Mg distribution coefficients between chlorite and chloritoid. They concluded that while the coefficients seem to approach unity as metamorphic grade increases, the range of values is limited, and chloritoid-chlorite distributions may be useful only as a relative geothermometer. Since the publication of

Table 4b. Average dolomite analyses.

Sample	B6	L6 r*	L6 c†	L7 r	L7 c	KP-2 r	MF-537 r	MF-551 r	MF-551 c	MF-647 r	MF-647 c
MgO	14.33	11.39	21.83	15.73	21.07	9.94	11.17	9.54	19.80	16.75	19.47
CaO	31.90	31.52	31.04	28.32	29.50	30.67	27.92	27.62	32.64	36.33	36.14
MnO	0.59	0.39	0.25	0.39	0.06	0.56	0.35	0.81	0.01	0.23	0.03
FeO ‡	8.25	11.69	0.33	7.07	0.07	15.61	16.28	17.60	0.73	3.09	0.32
Total	55.06	54.99	53.45	51.51	50.70	56.78	55.72	55.58	53.17	56.40	55.96
CO_2 §	45.57	44.77	47.60	46.05	47.70	44.12	44.29	43.84	47.28	46.40	47.10
Total	100.63	99.76	101.05	97.56	98.39	100.90	100.00	99.42	100.45	102.80	103.06
Fe^{2+}	0.219	0.321	0.008	0.197	0.002	0.427	0.450	0.497	0.019	0.078	0.008
Mg	0.679	0.558	0.982	0.781	0.995	0.484	0.551	0.480	0.907	0.749	0.853
Mn	0.016	0.011	0.006	0.011	0.002	0.015	0.010	0.023	0.000	0.006	0.001
Ca	1.086	1.110	1.004	1.011	1.001	1.074	0.989	0.999	1.075	1.168	1.138
Fe# ‖	0.244	0.365	0.008	0.201	0.002	0.469	0.450	0.509	0.020	0.094	0.009

Sample	MF-650 r	MF-736 r	MF-886 r	MF-889 r	MF-899 r	MF-900 r	MF-928	DrT 1210 r
MgO	9.97	15.04	14.22	14.13	11.74	13.06	21.66	14.61
CaO	30.26	30.12	29.20	28.74	29.41	30.31	31.37	30.10
MnO	0.88	0.17	0.63	0.32	0.81	0.37	0.22	0.34
FeO	13.69	10.30	11.04	11.71	15.57	11.26	2.76	11.43
Total	54.80	55.64	55.09	54.90	57.53	55.00	56.01	56.47
CO_2	44.29	45.52	45.28	45.24	44.40	45.09	45.40	45.31
Total	99.09	101.15	100.37	100.13	101.93	100.10	101.41	101.78
Fe^{2+}	0.385	0.272	0.297	0.316	0.415	0.305	0.067	0.299
Mg	0.500	0.707	0.681	0.680	0.558	0.631	0.472	0.682
Mn	0.025	0.005	0.017	0.009	0.022	0.010	0.003	0.009
Ca	1.090	1.017	1.005	0.995	1.005	1.053	0.491	1.010
Fe#	0.435	0.278	0.303	0.317	0.427	0.326	0.125	0.305

Note: * = rim; † = core; ‡ =All Fe as FeO; § = Assuming stoichiometric C; ‖ = Fe/(Fe+Mg)

Ghent *et al.* (1987), Holland & Powell (1990) have refined thermodynamic data for the Mg- and Fe-chlorite and chloritoid end members. These data now allow calculation of equilibrium temperatures from the analysis of chloritoid-chlorite K_d ($K_d = (Fe/Mg)_{Cld}/(Fe/Mg)_{Chl}$). In addition, Spear & Cheney (1989) reviewed Fe-Mg distributions between natural garnet-biotite and chloritoid-garnet pairs. From these data, and the fact that $(Fe/Mg)_{Bio}/(Fe/Mg)_{Chl} = 1$, the temperature dependence of chloritoid-chlorite K_d values can be calculated by an independent method. In addition, Vidal *et al.* (1999) revisited the possibility of calibrating the chloritoid-chlorite geothermometer. They had an advantage over earlier workers as many more data at lower temperatures were available.

Figure 2 is a plot of natural chloritoid-chlorite K_d values from the literature and their estimated formation temperatures. The data in solid black circles represent the data available to Spear & Cheney (1989) and earlier workers. Some of the temperatures were derived from other geothermometers (calcite-dolomite and biotite-garnet) but most were estimates based on limiting phase assemblages. The major sources of error in these temperatures are (1) uncer-

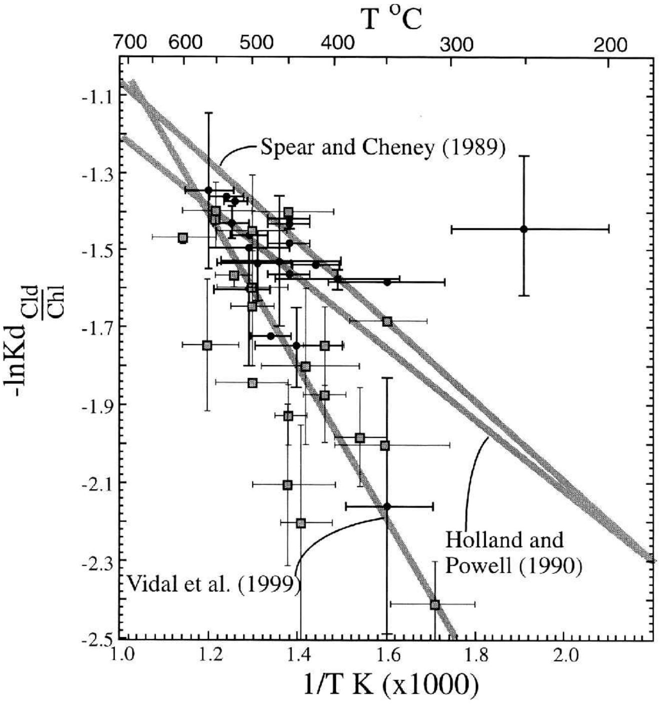

Fig. 2. Cld-Chl distribution coefficients plotted against estimated metamorphic temperatures. Data in solid circles from Frey *et al.* (1988), Grambling (1983), Banfield *et al.* (1989), Wang & Spear (1990), Chinner (1967), Cruickshank & Gent (1978), Paradis *et al.* (1983), Phillips (1988), Black (1975), Mposkos & Perdikatzis (1981), Albee (1972), Fox (1971 and 1975), Karabinos (1981), La Tour *et al.* (1980), Ashworth & Evirgen (1984), Ghent *et al.* (1987). Data in shaded squares from Vidal *et al.* (1999) their Table 1. The three lines are plots of the temperature dependence of Kd using the data of Spear & Cheney (1989), Holland & Powell (1990) and Vidal *et al.* (1999).

Table 5a. Temperature (°C) estimates from chloritoid-chlorite pairs.

Sample Location	MF-915 Gv	MF-920 Gv	MF-928 Gv	MF-931 Gv	MF-897 VG
S&C*	**290**	**250**	**250**	**260**	**370**
max	310	260	280	280	440
min	260	210	240	240	320
H&P†	**300**	**260**	**270**	**270**	**400**
max	330	280	300	300	500
min	280	210	250	250	350
VGBP‡	**420**	**390**	**400**	**400**	**480**
max	440	400	420	420	540
min	400	360	380	380	450
n §	6	4	4	6	12

Sample Location	MF-899 VG	MF-853 AT	MF-855 AT	MF-857 AT	DrT 1210 Sd
S&C	**700**	**370**	**410**	**410**	**390**
max	790	390	570	550	410
min	580	360	360	320	380
H&P	**850**	**400**	**460**	**460**	**440**
max	990	430	660	650	460
min	680	390	390	340	410
VGBP	**680**	**480**	**510**	**520**	**500**
max	720	500	610	600	510
min	620	470	480	450	490
n	5	6	71	58	6

Note: Average in boldface; * = using data of Spear and Cheney (1989); † = data of Holland and Powell (1993); ‡ = data of Vidal et al. (1999); § = number of mineral pairs; Gv = Gravera; VG = Val Gierm; AT = Alp Tgom; Sd = Sedrun

tainty about the activity of H_2O and (2) the use of end-member compositions for determining the positions of reactions in P-T space. Data from the Vidal *et al.* (1999) compilation are shown in shaded squares. Also plotted are lines representing the temperature dependence of the K_d calculated from the data of Spear & Cheney (1989) (SP), Holland & Powell (1990) (HP) and Vidal *et al.* (1999) (VGBP). The lines for SP and HP are similar at low temperatures and pass through most of the older data, especially at higher temperatures. However, the temperature dependence of VGBP differs greatly at low temperatures, while converging at higher temperatures. This is consistent with the addition of the new data. Table 5a lists the calculated temperatures for coexisting chloritoid-chlorite pairs from four locations in the epizone in the Urseren Zone. Sample MF-899 yields consistently anomalous temperatures regardless of which calibration is used. The reason for this is unknown. The low temperatures estimated for Gravera by the early calibrations are much higher using the VGBP estimate. In general, the VGBP calibration yields the highest temperatures of the three calibrations.

Carbonate minerals

Temperatures calculated from calcite-dolomite pairs calculated using the two equations of Bickle & Powell (1977) and one from Anovitz & Essene (1987) are given in Table 5b. The mean values (in bold type) from all three

Table 5b. Temperature (°C) estimates from calcite-dolomite pairs.

Sample Location	L6 Ld	L7 Ld	MF-650 Gg	MF-647 Gg	MF-551 Kp	MF-736 Pp	MF-928 Gv
B&P Cc*	**340**	**320**	**410**	**350**	**400**	**430**	**300**
max	420	460	470	380	620	570	450
min	270	210	360	330	280	360	150
n†	14	10	4	6	12	7	8
B&P Cc-Do‡	**340**	**450**	**400**	**340**	**380**	**430**	**360**
max	390	460	440	380	530	560	
min	270	430	350	310	270	360	
n	6	5	4	8	7	7	1
A&E Cc§	**280**	**320**	**380**	**310**	**320**	**410**	**220**
max	410	460	460	360	600	550	450
min	50	100	300	270	8	330	27
n	13	6	4	6	12	7	6

Sample Location	MF-886 VG	MF-889 VG	MF-899 VG	MF-900 VG	DrT 1210 Sd
B&P Cc	**470**	**470**	**510**	**470**	**460**
max	510	480	610	600	520
min	460	470	490	410	430
n	4	3	11	4	22
B&P Cc-Do	**460**	**460**	**480**	**450**	**440**
max	490	470	570	580	490
min	450	460	460	370	410
n	6	3	10	4	22
A&E Cc	**470**	**470**	**490**	**450**	**450**
max	500	470	560	570	500
min	450	460	470	390	420
n	4	3	11	4	22

Note: * = Bickle and Powell (1977) Mg and Fe in calcite; † = number of pairs; ‡ = Bickle and Powell (1977) Mg and Fe in calcite and dolomite; § = Anovitz and Essene (1987); Ld = Lindau; Gg = Guggenegg; Kp = Klausenpass; Pp = Panixierpass; Gv = Gravera; VG = Val Gierm; Sd = Sedrun

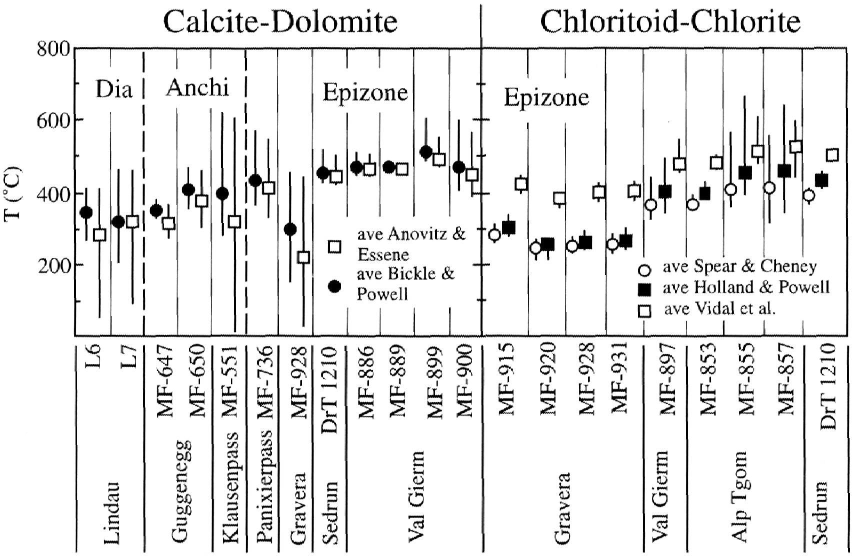

Fig. 3. Estimated temperatures from Cal-Dol geothermometers of Anovitz & Essene (1987) and Bickle & Powell (1977), temperatures from Fe–Mg distributions in chloritoid-chlorite. The range of Bickle & Powell (1977) temperatures include both Mg-Fe in calcite and dolomite-calcite calculations.

geothermometers are comparable but are generally higher for the two Bickle & Powell (1977) estimates than for those based on the geothermometer of Anovitz & Essene (1987).

Temperature variations

The mean values and ranges of temperatures from Tables 5a and b are plotted in Fig. 3. The results from both methods of Bickle & Powell (1977) are combined. Although calcite-dolomite temperatures increase with increasing grade (except for MF-928), the range in temperatures derived from the diagenetic samples overlaps those of the epizone. The data suggest that the range of estimated temperatures decreases as grade increases. This is consistent with disequilibrium in lower grades and the sluggish recrystallization rates of detrital carbonate minerals.

Calcite-dolomite estimates of the diagenetic samples from the Lindau borehole have a mean value around 300°C. This is much higher than the 100°C measured in the hole (Frey, 1978). Calcite-dolomite temperatures of the diagenetic zone do not differ much from the mean anchizone temperatures, which are between 300° and 400°C. The minimum temperature estimates from methane-rich fluid inclusions from other anchizone locations in the central Helvetic Nappes range between 250 and 264°C (Frey *et al.*, 1980b; Mullis, 1979). However, based on correlations between illite "crystallinity" (IC), mean vitrinite reflectance (Rm), and fluid composition data from the Kein and Lake Lucerne–Reuss valleys (Frey *et al.*, 1980b), rocks from Guggenegg and Klausenpass probably contain H_2O-rich inclusions and experienced higher-grade conditions than rocks with CH_4–bearing fluid inclusions. The calcite-dolomite temperatures for Guggenegg and Klausenpass in the anchizone are similar to temperatures (305–430°C) estimated for the Windgallen area at the northern rim of the Aar Massif (Frey *et al.*, 1980b).

Chloritoid-chlorite pairs from the epizone plot in three different groups. The samples from Gravera consistently record temperatures < 300°C for the SP and HP calibration, which is similar to results of calcite-dolomite thermometry. However, for these samples, the temperatures from the VGBP estimate are within the upper limit of the calcite-dolomite range. Samples from Alp Tgom and Sedrun have mean values around 400°C (SP, HP), somewhat lower than temperatures estimated from the carbonate minerals, and 500°C (VGBP), which is higher than carbonate estimates. Chloritoid-chlorite pairs in sample MF-897 record VGBP temperatures similar to those from the carbonate minerals from the same locality (Val Gierm), but sample MF-899 yields much higher chloritoid-chlorite temperatures regardless of calibration.

The estimated temperature for the epizone range from 250 to 510°C (SP, HP) or 390 to 520°C (VGBP)(mean values excluding MF-899). Estimates for most samples in Sedrun, Alp Tgom, and Val Gierm are similar to those of Frey *et al.* (1980a) (450°C), but SP and HP estimates for Gravera are much lower, while VGBP estimates are higher for other localities. The VGBP calibration is most likely more accurate at higher Fe contents, thus, yielding Gravera estimates more consistent with epizone conditions.

Thermodynamic data and analysis

The stability of low-temperature metamorphic minerals can be predicted from calculations using internally consistent thermodynamic databases (Berman, 1988; Holland & Powell, 1990). This is important in the study of low-grade metamorphic rocks which generally contain a paucity of geothermometers and indicators of grade. In addition, predicted mineral stabilities constrain equilibrium fluid compositions. Calculated petrogenetic grids are presented

Table 6. Abbreviations, formulae, and activity models used.

Symbol	Phase	Formula	Activity Model
An	anorthite	$CaAl_2Si_2O_8$	
And	andalusite	Al_2SiO_5	
ank	ankerite	$CaFe(CO_3)_2$	(X_{Fe})
Cal	calcite	$CaCO_3$	
chm	chamosite (daphnite)	$Fe_5Al[Si_3Al]O_{10}(OH)_8$	$16(X_{Fe,m1})^4(X_{Fe,m2})(X_{Al,m2})[X_{Al,t2}][X_{Si,t2}]$
cch	clinochlore	$Mg_5Al[Si_3Al]O_{10}(OH)_8$	$16(X_{Mg,m1})^4(X_{Mg,m2})(X_{Al,m2})[X_{Al,t2}][X_{Si,t2}]$
Chl	chlorite	$(Fe,Mg)_5Al[Si_3Al]O_{10}(OH)_8$	
Cld	chloritoid	$(Fe,Mg)Al_2SiO_5(OH)_2$	
cld	chloritoid	$FeAl_2SiO_5(OH)_2$	(X_{Fe})
Cz	clinozoisite	$Ca_2Al_3Si_3O_{12}(OH)$	
dol	dolomite	$CaMg(CO_3)_2$	(X_{Mg})
Dol	dolomite	$(Fe,Mg)Ca(CO_3)_2$	
fsd	ferrosudoite	$Fe_2Al_3[Si_3Al]O_{10}(OH)_8$	$256(X_{Fe,m1})^2(X_{Al,m1})^2(X_{Al,m2})(X_{vac,m2})[X_{Al,t2}][X_{Si,t2}]$
Gr	graphite	C	
Ky	kyanite	Al_2SiO_5	
Law	lawsonite	$CaAl_2Si_2O_7(OH)_2{\bullet}H_2O$	
Ma	margarite	$CaAl_2Si_3O_{10}(OH)_2$	
mcd	magnesiochloritoid	$MgAl_2SiO_5(OH)_2$	(X_{Mg})
Prl	pyrophyllite	$Al_2Si_4O_{10}(OH)_2$	
Qtz	quartz	SiO_2	
sud	sudoite	$Mg_2Al_3[Si_3Al]O_{10}(OH)_8$	$256(X_{Mg,m1})^2(X_{Al,m1})^2(X_{Al,m2})(X_{vac,m2})[X_{Al,t2}][X_{Si,t2}]$
Sud	sudoite	$(Fe,Mg)_2Al_3[Si_3Al]O_{10}(OH)_8$	

with the understanding that the uncertainty of the absolute positions of univariant curves increases with decreasing temperatures. However, the relative sequence of reactions in prograde metamorphism may be accurately predicted.

The data of Holland & Powell (personal communication, 1993, henceforth referred to as HP93) were chosen because they include data for Fe- and Mg-end-member chloritoid and dolomite and for sudoite. The minerals considered in the calculations and their abbreviations are listed in Table 6. Initially all the minerals available in the HP93 data base were included. The calculations predicted that magnesite and magnesiocarpholite were more stable than dolomite and chlorite. Because neither magnesite nor carpholite are present in the Liassic shales, these minerals were removed, and more reasonable assemblages were obtained.

The activity–composition model for chlorite is that of Holland & Powell (1990). Models for chloritoid and dolomite assume ideal mixing of Fe and Mg on one site. The entropy for ferrosudoite (the theoretical Fe end-member of sudoite) was estimated by the method of Holland (1989), with the addition of 35 J/mol configurational entropy. The enthalpy was calculated from the data of Theye *et al.* (1992) for sudoite-chlorite Fe–Mg distributions and assuming a temperature of 300°C. The heat capacity coefficient, a, was estimated from the relation: $a_{ferrosudoite} + a_{hematite} = a_{clinochlore} + a_{corundum} + a_{magnetite}$; thermal expansion and compressibility were assumed to be the same as sudoite. All estimated thermodynamic data are given in Table 7.

Margarite can have substantial solid solution with both paragonite and muscovite (Livi *et al.*, 1997). However, no mixing models have been established for these solutions. Simple ideal mixing calculations indicate that reduced activities of margarite to 0.8 would expand its stability field by approximately 10°C. In addition, the inclusion of a non-ideal model would increase margarite activity closer to unity. These calculations presented here assume unit activity of margarite, for lack of a better model.

Because organic matter is ubiquitous in the Liassic black shales and slates, and methane has been reported in high concentrations in fluid inclusions (Mullis, 1987; Mullis *et al.*, 1994), the fluid was assumed to be a graphite-buffered C-O-H mixture. The modified Redlich-Kwong equation of state (EOS) of Connolly & Cesare (1993) was used to calculate fluid properties and speciation. At the pressures and temperatures of interest (200–500°C and 1.5–3 kbar), both

Table 7. Thermodynamic data for sudoite end-members.

phase	S°_{298} J/(mol K)	$\Delta H_f{}^{\circ}_{298}$ kJ/mol	V°_{298} kJ/(mol kbar)	αV K^{-1}(x 10^{-5})	βV $kbar^{-1}$(x 10^{-3})
sud	399	-8636.010	203	56.0	29.0
fsd	457	-7911.003	204.7	56.0	29.0

phase	a* kJ/(mol K)	b* kJ/(mol K) (x 10^{-5})	c* kJ/(mol K)	d* kJ/(mol K)
sud	1.4361	4.8749	-2748.5	-13.764
fsd	1.1904	0.28	-6582.7	-11.101

Note: * = heat capacity coefficients.

Ferry & Baumgartner (1987) and Connolly & Cesare (1993) predicted that metamorphic fluids are nearly binary CH_4-H_2O or H_2O-CO_2 solutions. Therefore, the fluids may be considered to be simple binary mixtures to a good approximation. The calculations presented below do not assume such binary behavior and estimate concentrations of all species at all relevant temperatures and pressures. However, for the purposes of discussion, the fluids will be referred to as simple binary mixtures.

The crystallization of graphite from organic matter is not complete in the low-grade Central Alps (Hoefs & Frey, 1976, report organic matter as "badly crystallized graphite" in the Urseren Zone). A possible complication in the model presented here is that the activity of graphite in the organic matter described as "poorly crystallized" graphite may deviate significantly from unity. If the carbonaceous material is metastable with respect to well crystallized graphite, the activity of graphite appropriate for the model would be greater than unity. For water-rich fluid compositions, such a deviation would tend to raise the activity of carbonic fluid species at the expense of water activity, and thus, destabilize hydroxylated silicates. However, the persistence of poorly crystallized carbonaceous matter in high grade metamorphic rocks (*e.g.*, Buseck & Huang, 1985; Large *et al.*, 1994), suggests that at least some carbonaceous material is essentially inert, and therefore, the effective activity of graphite in systems containing such material may be below unity. The potential effects of this were modeled by reducing the activity of graphite to as low as 0.25. Variations in graphite activity had little effect on the calculated positions of the univariant equilibrium curves. Given this qualitative and quantitative uncertainty, we assume unit activity of graphite as the least arbitrary model. Therefore, the calculations presented here are for unit activity of graphite.

Following the procedure of Connolly & Cesare (1993), fluid compositions are represented by the atomic fraction of oxygen relative to hydrogen in the fluid, $X_O = n_O/(n_O+n_H)$). Thus, pure H_2O has $X_O = 1/3$. H_2O-CO_2 mixtures have $X_O > 1/3$, whereas CH_4-H_2O mixtures have $X_O < 1/3$. In simple binary H_2O-CO_2 and CH_4-H_2O solutions, the estimation of mole fraction (y) of species i in the fluid can be obtained by the equations

$$y_{CO_2} = \frac{3X_O - 1}{X_O + 1}, \text{ for } X_O > \frac{1}{3}$$

$$y_{CH_4} = \frac{1 - 3X_O}{X_O + 1}, \text{ for } X_O < \frac{1}{3}.$$

Calculation of the phase equilibria was performed with the computer program PERPLEX (Connolly & Kerrick,

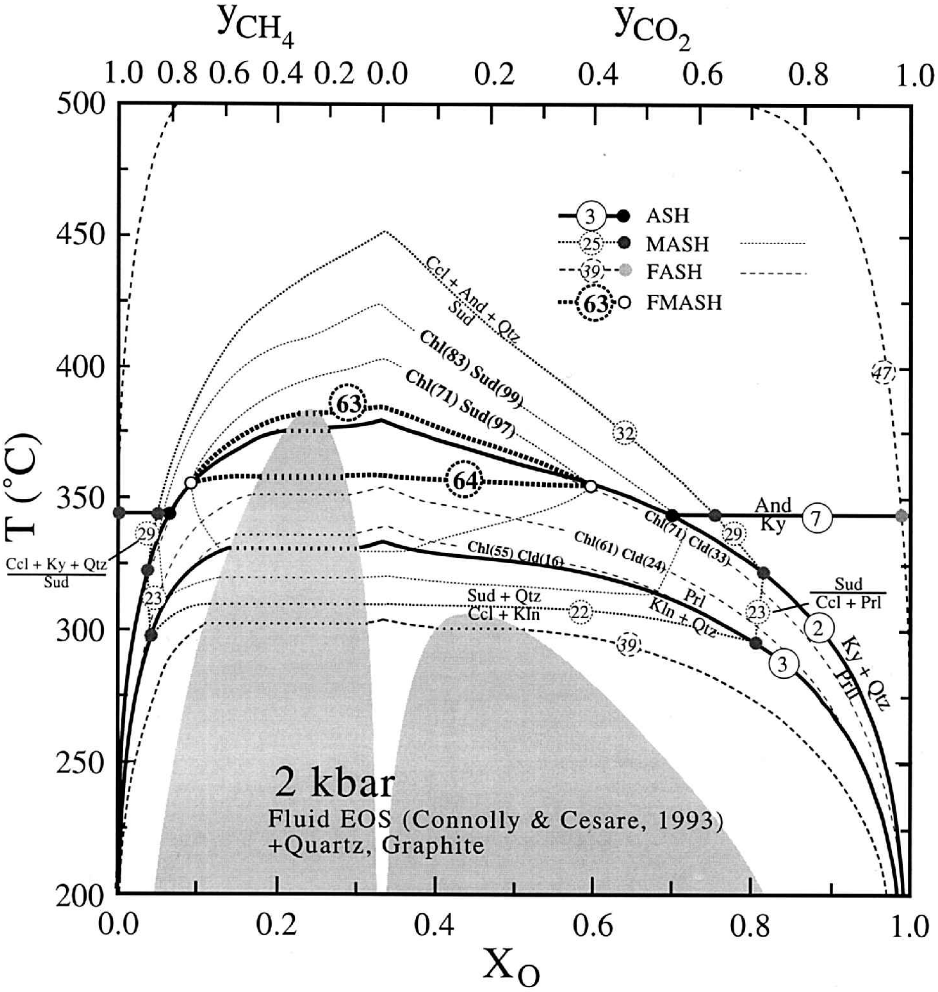

Fig. 4. FMASH mineral relations calculated using the data of Holland & Powell (1993, pers. comm.). Circled numbers refer to reactions in Table 7. Is1 and Is2 are invariant points terminating reaction [24a].

$$X_O = n_O/(n_O+n_H),$$

$$y_{CO_2} \approx \frac{3X_O - 1}{X_O + 1}, \text{ for } X_O > \frac{1}{3},$$

$$y_{CH_4} \approx \frac{1 - 3X_O}{X_O + 1} \text{ for } X_O < \frac{1}{3},$$

see text for further explanation. Lightest weight dashed lines are traces of divariant reactions labeled by the Fe-Mg bearing minerals. Numbers in parentheses are molar Mg/(Mg + Fe) × 100%. Shaded portions of the diagram are the fluid miscibility gap based on the equation of Connolly & Cesare (1993).

1987). Previous calculations of low-temperature petrogenetic grids the CASH system have been attempted by Frey (1987a) using the Berman data base, and Ranson (2000) using the Holland & Powell data. Vidal *et al.* (1992 and 1999), employing Berman (1988) and their own thermodynamic data, considered portions of the CMASH system at high pressures. Giorgetti *et al.* (1998) investigated P-T relations in FMASH and KMASH using a similar data base. In the present paper, T-X_O diagrams for the CFMASH (silica- and graphite-buffered) system and degenerate systems evaluated over the entire range of X_O including consideration of solid solution in Fe-Mg minerals. A pressure of 2 kbar was chosen to represent the anchizone in the Glarus Alps region, and 3 kbar for the epizone in the Urseren Zone (Frey *et al.*, 1980a).

T-X_O phase relations in the system FMASH

Calculations in the system FMASH (Fig. 4) include equilibria between the Fe-Mg minerals chlorite, sudoite, and the aluminosilicates kaolinite, pyrophyllite, kyanite, and andalusite. Calculations consider that chlorite, sudoite, and chloritoid are ideal Fe–Mg solid solutions. The activity models are listed in Table 6 along with that of dolomite, and the equilibria are given in Table 8. This diagram is applicable to carbonate-poor aluminous shales. The shaded portion of Fig. 4 delineates the two-phase region for CH_4-H_2O and H_2O-CO_2 fluids. The reaction Prl + Chm = Cld + Qtz + H_2O is not present in Fig. 4 because it is metastable with respect to reactions involving kaolinite [39] in FASH. Frey (1987a) discussed whether chloritoid exists at low temperatures and cites some evidence for chloritoid in the anchizone. However, Kln + Cld is very rare. This may be related to the rarity of very Fe-rich shales or that formation of chloritoid from kaolinite is kinetically inhibited. Rocks containing more Mg will produce chloritoid from the divariant reactions Prl + Chl = Cld + Qtz + H_2O and are labeled with chlorite and chloritoid with % Mg end-member. The HP93 data predict no stability field for

Table 8a. CASH reactions.

#	Reaction*
1	Cal + Kln = Law + CO_2
2	Prl = Ky + Qtz + H_2O
3	Kln + 2 Qtz = Prl + H_2O
4	Cal + 2 Kln = Ma + 2 Qtz + 3 H_2O + CO_2
5	Cal + 2 Prl = Ma + 6 Qtz + H_2O + CO_2
6	Cal + 2 Ky + H_2O = Ma + CO_2
7	Ky = And
8	Cal + 2 And + H_2O = Ma + CO_2
9	5 Cal + 3 Ma + 6 Qtz = 4 Cz + H_2O + 5 CO_2
10	Cal + Ma + 2 Qtz = 2 An + H_2O + CO_2
11	Cal + And + Qtz = An + CO_2
12	Ma + Qtz = An + And + H_2O
13	2 Cz + CO_2 = Cal + 3 An + H_2O
14	Ma + 2 Cz + 2 Qtz = 5 An + 2 H_2O
15	Prl = And + Qtz + H_2O
16	Ma + Qtz = An + Ky + H_2O
17	5 Law = Ma + 2 Cz + 2 Qtz + 8 H_2O
18	Kln + Law = Ma + 2 Qtz + 3 H_2O
19	4 Ma + 3 Qtz = 2 Cz + 5 Ky + 3 H_2O
20	Cal + 3 Law + CH_4= 2 Cz + 7 H_2O + 2 C

Note: * = High-temperature assemblage on right.

Table 8b. CMASH reactions.

#	Reaction*
21	5 Dol + Kln + Qtz + 2 H_2O = 5 Cal + Cch + 5 CO_2
22	2 Cch + 8 Kln = 5 Sud + 7 Qtz + 4 H_2O
23	2 Cch + 8 Prl + 4 H_2O = 5 Sud + 23 Qtz
24	2 Dol + 2 Kln = 2 Cal + Sud + Qtz + 2 CO_2
24a	2 Dol + 2 Prl + 2 H_2O = 2 Cal + Sud + 5 Qtz + 2 CO_2
25	8 Dol + Sud + 3 Qtz + 3 H_2O = 8 Cal + 2 Cch + 8 CO_2
26	4 Cal + 5 Sud = 2 Cch + 4 Ma + Qtz + 8 H_2O + 4 CO_2
27	2 Dol + Ma + Qtz + 3 H_2O = 3 Cal + Sud + CO_2
28	2 Dol + 6 Prl = Sud + 2 Ma + 17 Qtz + 4 CO_2
29	8 Sud = 2 Cch + 8 Ky + Qtz + 12 H_2O
30	Sud + 2 Ma + 4 CO_2 = 2 Dol + 6 And + Qtz + 6 H_2O
31	8 Dol + 11 Sud + Qtz = 6 Cch + 8 Ma + 12 H_2O + 16 CO_2
32	5 Sud = 2 Cch + 8 And + Qtz + 12 H_2O
33	5 Dol + 11 And + 2 Qtz + 9 H_2O = Cch + 5 Ma + 10 CO_2
34	10 Dol + Ma + 4 Qtz + 7 H_2O = 11 Cal + 2 Cch + 9 CO_2
35	5 Dol + 6 Ma + 13 Qtz = Cch + 11 An + 2 H_2O + 10 CO_2
36	5 Dol + And + 7 Qtz + 4 H_2O = Cch + 5 An + 10 CO_2
37	5 Dol + An + Qtz + 4 H_2O = 6 Cal + Cch + 4 CO_2

Note: * = High-temperature assemblage on right.

Table 8c. CFASH reactions.

#	Reaction*
38	Kln + 5 Ank + Qtz + 2 H_2O = 5 Cal + Chm + 5 CO_2
39	4 Kln + Chm = 5 Cld + 6 Qtz + 7 H_2O
40	Kln + Ank = Cal + Cld + Qtz + H_2O + CO_2
41	Ank + Prl = Cal + Cld + 3 Qtz + CO_2
42	Ank + 3 Prl = Ma + Cld + 9 Qtz + H_2O + 2 CO_2
43	2 Cal + 5 Cld + 2 Qtz + H_2O = Chm + 2 Ma + 2 CO_2
44	Cld + 4 Ank + 2 Qtz + 3 H_2O = 4 Cal + Chm + 4 CO_2
45	Ma + 2 Ank + H_2O = 3 Cal + 2 Cld + CO_2
46	Ank + 3 Ky + 2 H_2O = Ma + Cld + 2 CO_2
47	5 Cld + 2 Qtz = Chm + 4 Ky + H_2O
48	Ma + 10 Ank + 4 Qtz + 7 H_2O = 11 Cal + 2 Chm + 9 CO_2
49	11 Cld + 4 Ank + 6 Qtz + 5 H_2O = 3 Chm + 4 Ma + 8 CO_2
50	Ank + 3 And + 2 H_2O = Ma + Cld + 2 CO_2
51	6 Ma + 5 Ank + 13 Qtz = Chm + 11 An + 2 H_2O + 10 CO_2
52	2 Ma + Ank + 3 Qtz = 3 An + Cld + H_2O + 2 CO_2
53	5 Cld + 2 Qtz = Chm + 4 And + H_2O
54	Ank + 2 And + Qtz + H_2O = An + Cld + 2 CO_2
55	3 Cld + 2 Ank + 4 Qtz + H_2O = Chm + 2 An + 4 CO_2
56	An + 5 Ank + Qtz + 4 H_2O = 6 Cal + Chm + 4 CO_2
57	Chm + 4 Ma + 2 Qtz = 4 An + 5 Cld + 3 H_2O
58	8 Cz + 5 Cld + 6 Qtz = Chm + 16 An + 5 H_2O
59	5 Chm + 16 Ma + 2 Qtz = 8 Cz + 25 Cld + 7 H_2O
60	4 Law + 5 Cld = Chm + 4 Ma + 2 Qtz + 5 H_2O
61	Chm + 16 Law = 8 Cz + 5 Cld + 6 Qtz + 27 H_2O

Note: * = High-temperature assemblage on right.

Table 8d. CFMASH reactions.

#	Reaction*	Singular points
62	Dol + Kln + Sud + Qtz + H_2O ≈ Cal + Ma + Chl + CO_2	many
63	Dol + Kln + H_2O ≈† Cal + Chl + Cld + Qtz + CO_2	many
64	Dol + Kln ≈ Ma + Cld + Qtz + H_2O + CO_2	many
65	Dol + Kln + Sud ≈ Ma + Chl + Qtz + H_2O + CO_2	many
66	Dol + Prl = Cld + Chl + Ma + Qtz + H_2O + CO_2	
67	Dol + Prl + Sud = Chl + Ma + Qtz + H_2O + CO_2	
68	Dol + Sud + Qtz + H_2O ≈ Cal + Chl + Ma + CO_2	many
69	Prl + Chl = Sud + Cld + Qtz + H_2O	
70a	Dol + Ma + Qtz + H_2O = Cal + Chl + Cld + CO_2	I_{13}-a
70b	Dol + Ma + Cld + Qtz + H_2O = Cal + Chl + CO_2	a-b
70c	Dol + Ma + Qtz + H_2O = Cal + Chl + Cld + CO_2	b-I_3
71	Sud + Cld + Qtz = Chl + Ky + H_2O	
72	Dol + And + Qtz + H_2O = Cld + Chl + An + CO_2	
73	Dol + Ma + Qtz = Cld + Chl + An + H_2O + CO_2	
74	Dol + And + Qtz + H_2O = Cld + Chl + Ma + CO_2	
75	Dol + Prl = Cld + Chl + Ma + Qtz + H_2O + CO_2	
76	Dol + Cld + Sud + Qtz + H_2O = Chl + Ma + CO_2	
77	Dol + Ky + Qtz + H_2O = Sud + Cld + Ma + CO_2	
78	Dol + Ky + Sud + Qtz + H_2O = Chl + Ma + CO_2	
79	Dol + Ky + Qtz + H_2O = Cld + Chl + Ma + CO_2	
80	Sud + Cld + Qtz = Chl + And + H_2O	

Note: * = High-temperature assemblage on right; †≈ = Reaction written with dominant stoichiometric signs.

magnesiochloritoid at 2 kbar. This agrees with the observations of Chopin & Schreyer (1983) that magnesiochloritoid is stable only at high pressures. Pure sudoite forms at the lowest temperatures by reaction [22] involving kaolinite. Formation of sudoite from pyrophyllite occurs by reaction [23]. This reaction was also predicted by Giorgetti *et al.* (1998) using an augmented Berman data base. The addition of Fe to chlorite and sudoite restricts the range of X_O of the divariant assemblage Prl + Sud + Chl + Qtz + Gr + fluid (see contours in Fig. 4). The divariant reaction involving chlorite and sudoite or chloritoid are truncated by the FMASH invariant reactions [69] and [80].

The compositional changes of chlorite, sudoite, and chloritoid as a function of temperature are best illustrated by the diagram in Fig. 5. This T-$X_{(Fe)}$ section is taken at a fluid composition and pressure estimated for anchimetamorphism in the Northern Glarus Alps. The calculation of this diagram assumes that the system is buffered with

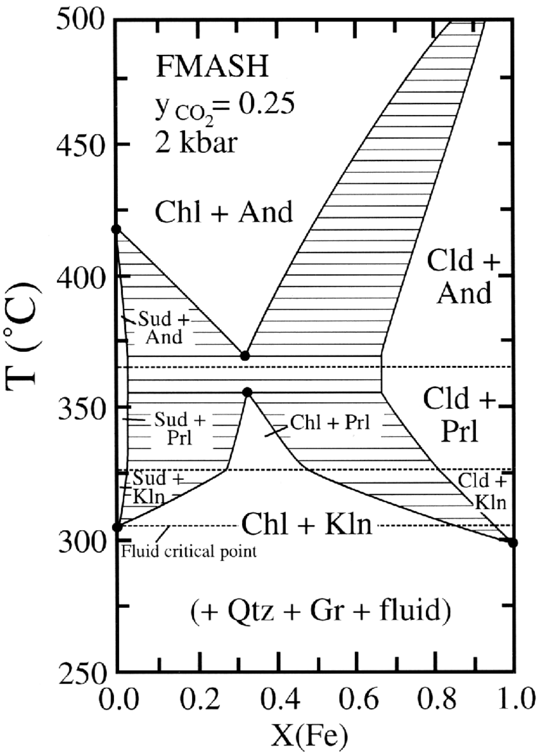

Fig. 5. Plot of temperature verses composition of Fe-Mg minerals in the system FMASH with quartz, graphite, and an aluminosilicate phase present, and for the fluid composition of y_{CO_2} = 0.25. Horizontal dashed lines are temperatures for reactions in the buffered phases.

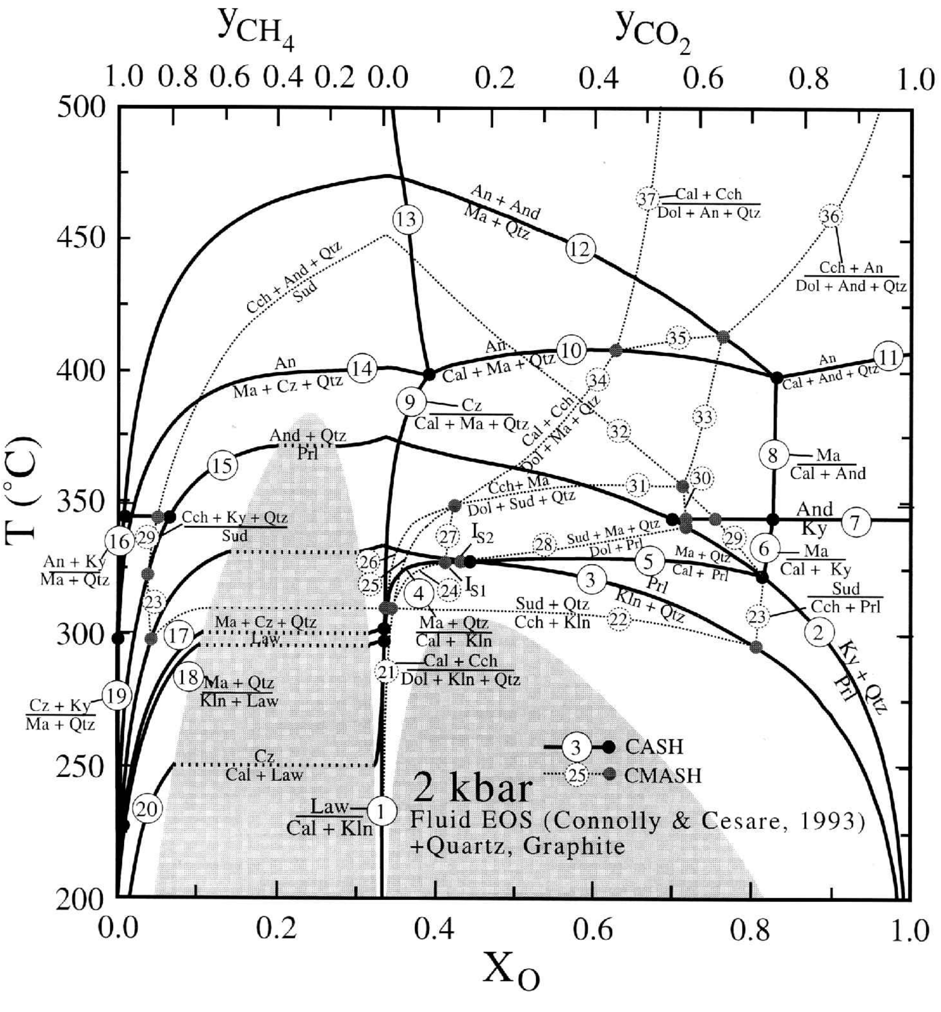

Fig. 6. CMASH mineral relations along with the calculated fluid miscibility. Numbers refer to CASH and CMASH reactions in Table 7.

respect to SiO_2 and Al_2O_3 by the presence of quartz and an aluminosilicate phase, and the fluid is buffered by graphite. The thermodynamic data for sudoite predict little solid solution of Fe in sudoite. Analyses for sudoite from the Liassic shales contain more Fe than predicted. This is an indication that the thermodynamic data for sudoite in the HP data base needs further refinement. The range for Mg solid solution in chloritoid is greater and has a maximum Mg content when coexisting with sudoite. Invariant points on Fig. 5 correspond to invariant curves in Fig. 4. The addition of Ca to the system makes the low-temperature assemblage Chl + Kln + Qtz + Gr + fluid metastable with respect to Dol + Cal + Kln + Qtz + Gr + fluid and changes the low-temperature reactions which form sudoite and chloritoid. These reactions are discussed in the next sections.

T-X_O phase relations in the system CASH

Calculated equilibria in the system CASH are plotted as solid curves in Fig 6. The positions of reaction curves and invariant points on the side of the diagram at $X_O > 1/3$ are qualitatively similar to those predicted by Frey (1987a) using the data of Berman (1988). One important difference is that the Prl + Cal stability field between the reactions Cal + Prl = Ma [5] (reaction number is given in square brackets) and Kln = Prl [3] has a much narrower temperature range than that predicted by the Berman (1988) data.

Reaction curves involving calcite do not cross a divide at $X_O = 1/3$ ([4], [9], [13], and [20]). Thus, $X_O = 1/3$ is not only a boundary in fluid composition, but also a boundary in mineral stability. The stability fields for calcite coexisting with margarite and anorthite are incompatible with fluids containing significant methane. Similarly, Cal + Law or Cal + Cz are compatible only with methane-rich or H_2O-rich fluids. The assemblage Ma + Cal, defined by reactions [4] through [10], is stable from 310–405°C and is an index assemblage for the epizone. However, reduced activities of margarite and anorthite will effect these limits.

The assemblage Prl + Cal (bounded by [2], [3], and [5]) is not uncommon in Liassic shales from the anchizone. Frey (1978) determined by X-ray powder diffraction that 13% of rocks from the anchizone contained Prl + Cal. This is a minimum value because X-ray powder diffraction only detects calcite and pyrophyllite if they are ≥ 5% by volume. Almost all shales investigated from the Quartenschiefer, Triassic redbeds associated with the Liassic, contain carbonate minerals (Sharp *et al.*, 1995). This assemblage is important for its chemical simplicity and narrow temperature range of stability at high to intermediate y_{CO_2} values. It also commonly defines the middle to upper anchizone in

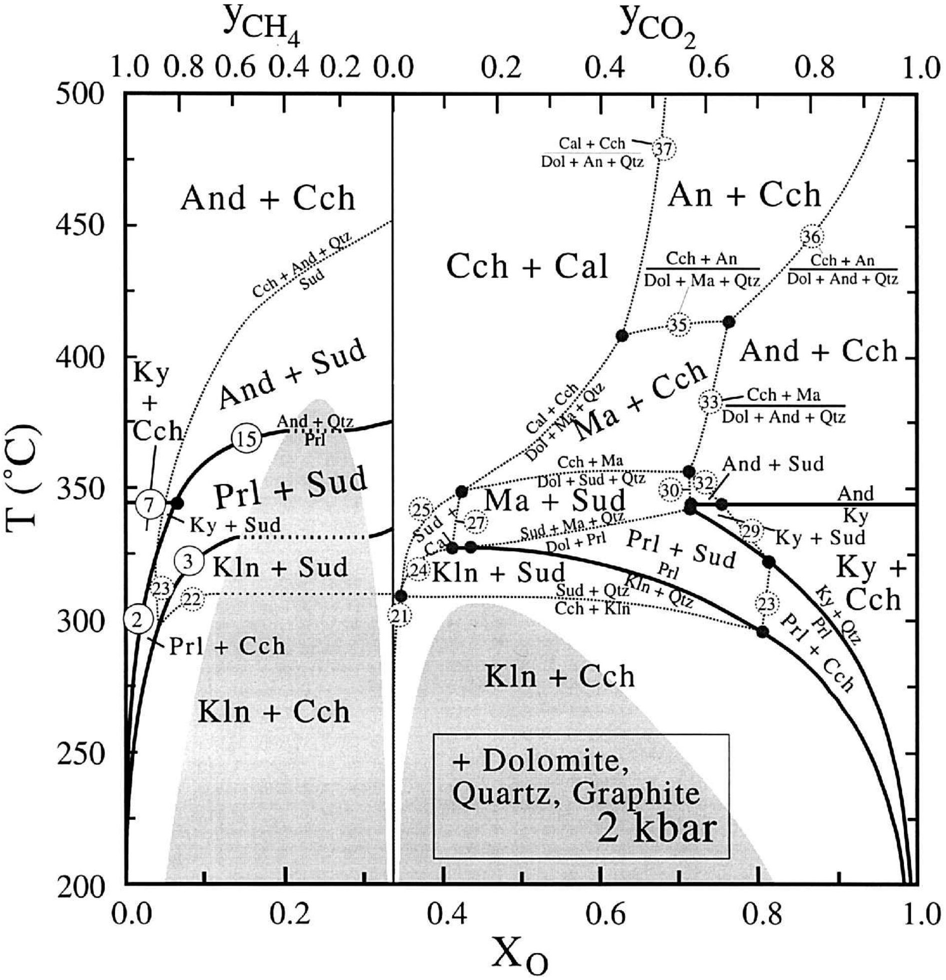

Fig. 7. Stability fields for mineral assemblages in the system CMASH at 2 kbar for metamorphic equivalents of the model assemblage Kln + Cch + Dol + Qtz + Gr. All assemblages contain calcite, dolomite, quartz, and graphite in excess. Curves are the same as in Fig. 6.

aluminous slates (Frey, 1987a and b). The minimum y_{CO_2} value for this assemblage is ~ 0.1 at a maximum temperature of 325°C at 2 kbar. The temperature range of stable Prl + Cal increases as pressure increases (see below). However, this assemblage is also reflected in the $X_O > 1/3$ region and has a large temperature and fluid composition range.

Of the 15 CASH reactions in the region $X_O > 1/3$, only 6 are dehydration reactions. Most reactions in this region produce volatile mixtures with $X_O \geq 0.55$. Where $X_O < 1/3$, all reactions involve dehydration, except for [20], and all reactions including [20] drive metamorphic fluid compositions toward the $X_O = 1/3$ boundary.

T-X_O phase relations in the system CMASH

Equilibria in the CMASH system appear as dotted lines in Fig. 6. A T-y_{CO_2} petrogenetic grid for this system at 5 kbar was calculated by Baker *et al.* (1994) using the data of HP90 but for higher temperatures and fluid compositions restricted to $X_O > 1/3$. The results listed below compliment their observations.

The stable low-temperature (200°C) SiO_2-Al_2O_3-CaO buffered assemblage is Dol + Kln + Cal + Qtz and chlorite is not stable over most values of y_{CO_2}. Thus, low temperature formation of sudoite consumes dolomite. However, the reaction Kln + 5 Dol + Qtz + 2 H_2O = Cch + 5 Cal + 5 CO_2 [21] will produce chlorite in H_2O-rich fluid regimes and can change the reactants available for the formation of sudoite, chloritoid and margarite. Reactions involving dolomite are restricted to the CO_2 side of $X_O = 1/3$ (see [24], [25], and [26] Table 8).

Mineral stability fields in Fig. 7 depict prograde metamorphism of a model rock containing quartz, dolomite, kaolinite, and clinochlore. The system is not buffered with respect to CaO, and therefore, dolomite and clinochlore can coexist. The minerals quartz, kaolinite, and chlorite commonly coexist in diagenetic-grade aluminous shales. The presence of dolomite may occur more frequently than reported because they are often ignored or are present in low abundances. The abundance of kaolinite in the protolith is greater than four times that of clinochlore to maintain saturation with respect to Al_2O_3. For the region $X_O < 1/3$ in Fig. 7, no reactions with carbonates are predicted.

With the exception of Cch + Kln = Sud [22] and Cch + Prl = Sud [23], all sudoite-forming reactions in CMASH involve dolomite. The mineral stabilities predicted in Fig. 7 indicate that sudoite should be common in Mg-rich, aluminous shales at 2 kbar and temperatures above 300°C. At 2 kbar, the assemblage Prl + Sud + Dol ± Cal is stable over a

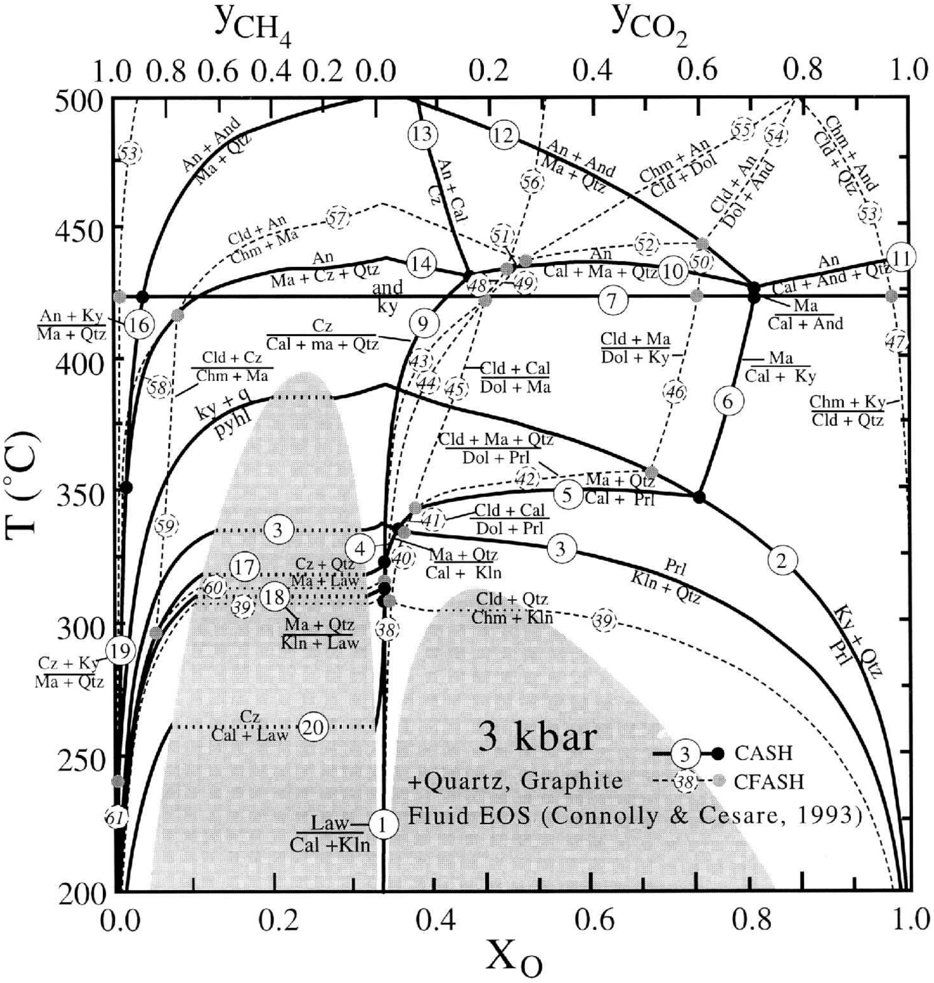

Fig. 8. CFASH mineral relations. Numbers refer to CASH and CFASH reactions in Table 7.

limited temperature range of approximately 300–340°C coexisting with fluids of intermediate y_{CO_2} values. The assemblage Prl + Cch + Dol extends to low temperatures, and indicates high y_{CO_2} or y_{CH_4}. The assemblage Ma + Sud + Dol is stable only over the temperature range 325–350°C. As in the case of CASH reactions (except [20]), CMASH reactions involve dehydration at $X_O < 1/3$. Of the sixteen CMASH reactions, only four are dehydration reactions. Thus, there is a tendency for mineral reactions to drive fluids to CO_2-rich compositions in Mg-rich aluminous shales when $X_O > 1/3$.

T-X_O phase relations in the system CFASH

The T-X_O diagram for the CFASH system (Fig. 8, Table 8c) was calculated for 3 kbar to simulate metamorphism in the epizone of the Urseren Zone, where formation of Fe-rich chloritoid is important. Calculated mineral stabilities for prograde metamorphism of a model protolith with Kln + Chm + Ank + Qtz + Gr (Kln/Chm ≥ 4) are presented in Fig. 9. In shales containing carbonate minerals and abundant aluminosilicate, margarite is not stable in pure H_2O fluids, but is confined to intermediate y_{CO_2} values (~ 0.05–0.6) and temperatures between 340 and 440°C at 3 kbar. In the region $X_O < 1/3$, prograde metamorphism produces similar mineral sequences as the CMASH system but substituting chloritoid for sudoite.

Of the nineteen reactions at $X_O > 1/3$ in Fig. 8, only four are dehydration reactions. Thus, as in the CMASH system, prograde reactions typically drive fluids to greater y_{CO_2}. Similarly, there is no mechanism for increasing the CH_4 content of the fluid through mineral reactions. This has important implications for the diagenetic and low-anchizone shales that contain CH_4-rich fluid inclusions (Mullis *et al.*, 1994). The presence of CH_4 would have the effect of suppressing most reactions between silicate and carbonate minerals. Margarite is found in the Liassic shales and fluids coexisting with these rocks could not have been CH_4-rich. If at lower grades the fluid was, in fact, CH_4-rich, three mechanisms are possible for the change to fluid compositions inferred at higher grades: (1) oxidation of CH_4, (2) increasing H_2O contents by dehydration reactions, (3) infiltration of rock by an externally-derived H_2O-CO_2 fluid. No evidence for oxidation reactions has been observed. In the Liassic shales, the only possible dehydration reaction in the anchizone is Kln + 2 Qtz = Prl + H_2O [3]. In some rocks, the abundance of kaolinite may have been great enough to dilute CH_4, but the fluid must also become an H_2O-CO_2 mixture for margarite to be stabilized. Therefore, some CO_2 must be added. No diagenetic

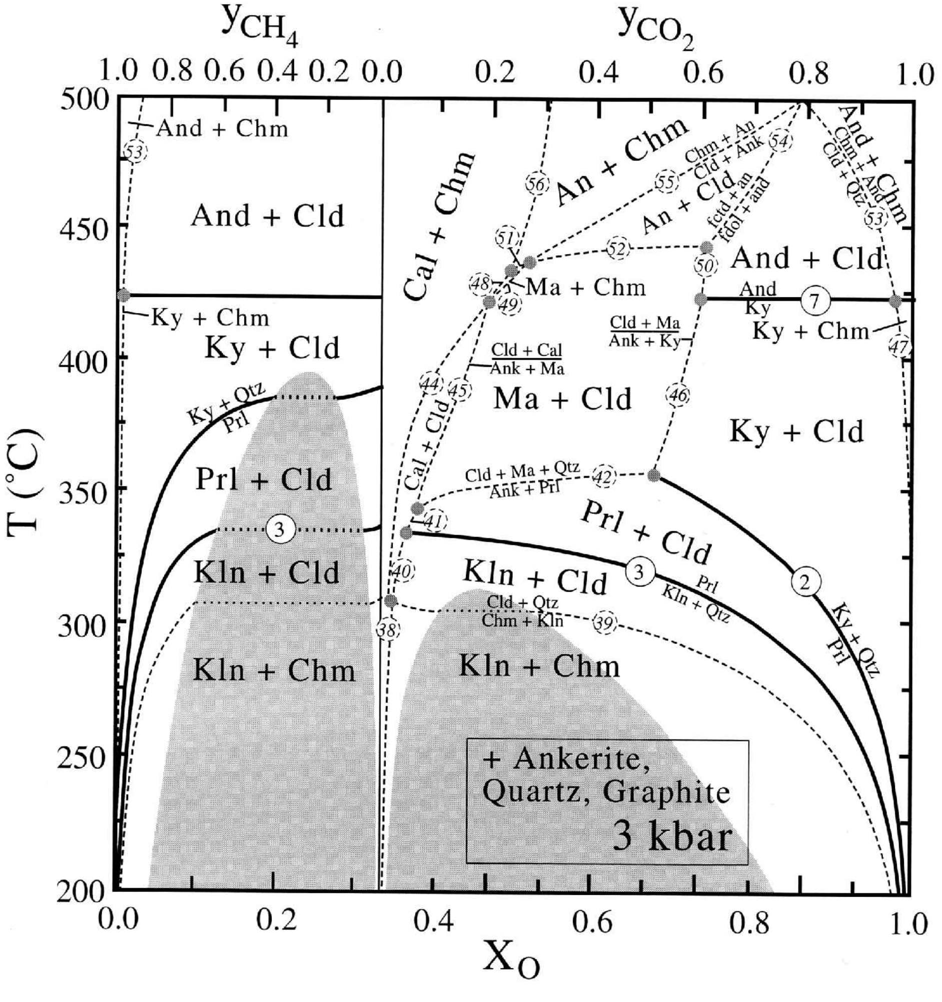

Fig. 9. Stability fields for mineral assemblages in the system CFASH at 3 kbar for metamorphic equivalents of the model assemblage Kln + Chm + Ank + Qtz + Gr. All assemblages contain ankerite, quartz, and graphite in excess.

mineral reactions predicted from the HP93 data base produce CO_2. However, maturation of organic matter might produce CO_2. It is possible to test for fluid infiltration, and evidence for it is presented later.

T-X_O phase relations in the system CFMASH

The diagram for the CFASH system is of limited use because the addition of Mg causes important changes in the reactions forming sudoite and chloritoid. Therefore, the system CFMASH has been calculated and presented in a series of diagrams that simplify this complex reaction space. Discussion of the reactions will be limited to those that pertinent to the metamorphic conditions of the Central Alps.

Several features of these calculations are important to note. (1) The CASH reactions are still univariant since they do not include Fe-Mg minerals. (2) All other univariant reactions involve three solid solutions. (3) Because solid solution compositions adjust to changes in T and X, the stoichiometry of the reactions continuously changes. Therefore, the exact stoichiometry cannot be listed in Table 8d. (4) The changing mineral compositions also may cause phases to switch from being reactants to being products. The point at which a reactant becomes a product or *vice versa* is a singular point (Abart *et al.*, 1992; Shreinemakers, 1924). These singular points are denoted as "a" and "b" and the reactions between singular points are listed in Table 8d. (5) Many of the univariant CFMASH reactions terminate at degenerate invariant points (IP).

Univariant reactions in CFMASH

Univariant reactions are drawn in heavy dashed lines in Fig. 10a and are separated for clarity in Fig. 10b through d. Rapid changes in the sign of stoichiometric coefficients of participants in [62], [63], [64], and [65] were found, which may be an artifact of Perplex where a univariant reaction approaches a degenerate invariant point. For these reasons, the calculated reaction stoichiometries are not reported for univariant reactions in Table 8. Tick marks on the univariant curves in Fig. 10b through d indicate chlorite compositions in Mg/(Mg + Fe) × 100%. All Fe-Mg minerals change in the same sense (*e.g.*, increasing Fe) along a reaction. The incremental values of chlorite can be used to link divariant reactions that operate between univariant reactions. From calculated values of chlorite composition, their temperatures, and the thermodynamic data from HP93, K_d values and mineral compositions of the other products and reactants can be estimated. Invariant point assemblages and

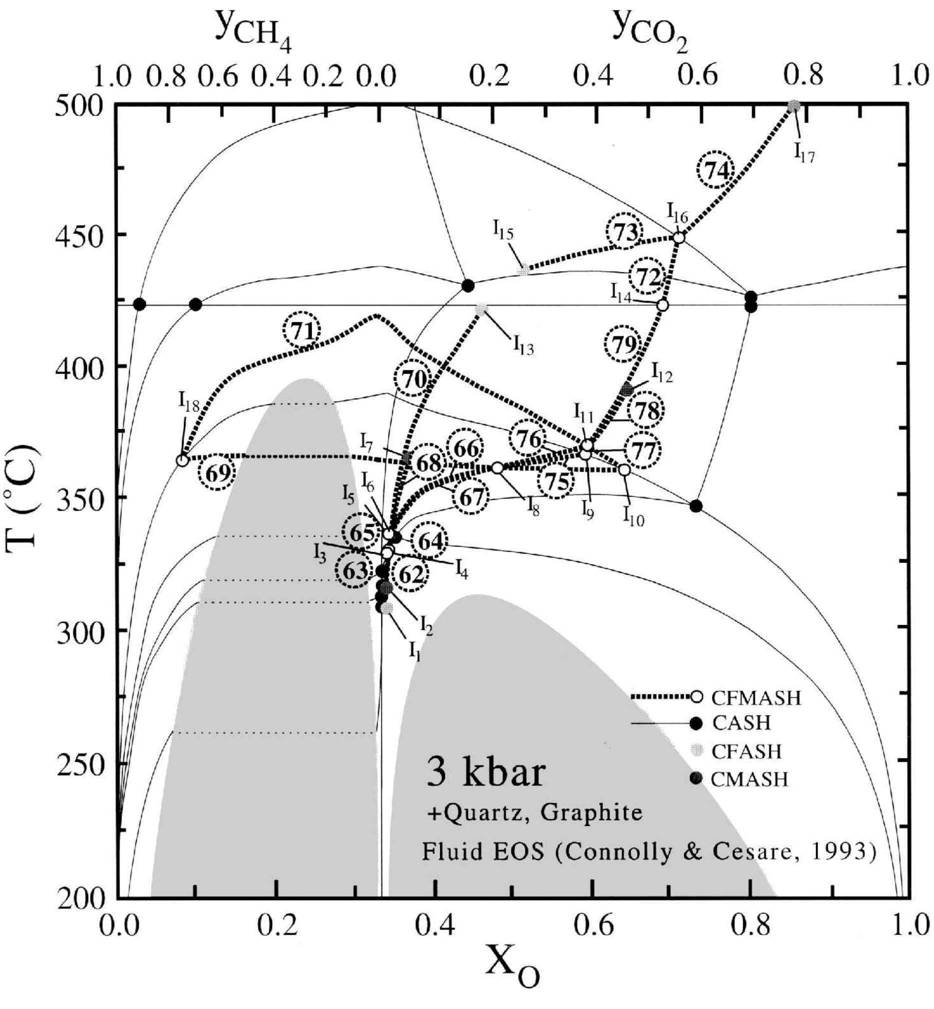

Fig. 10a. CFMASH mineral relations calculated at 3 kbar. Circled numbers refer to CFMASH equilibria (bold dashed lines) in Table 7d. CASH curves as in Fig. 8. I_1–I_{17} are invariant points listed in Table 8.

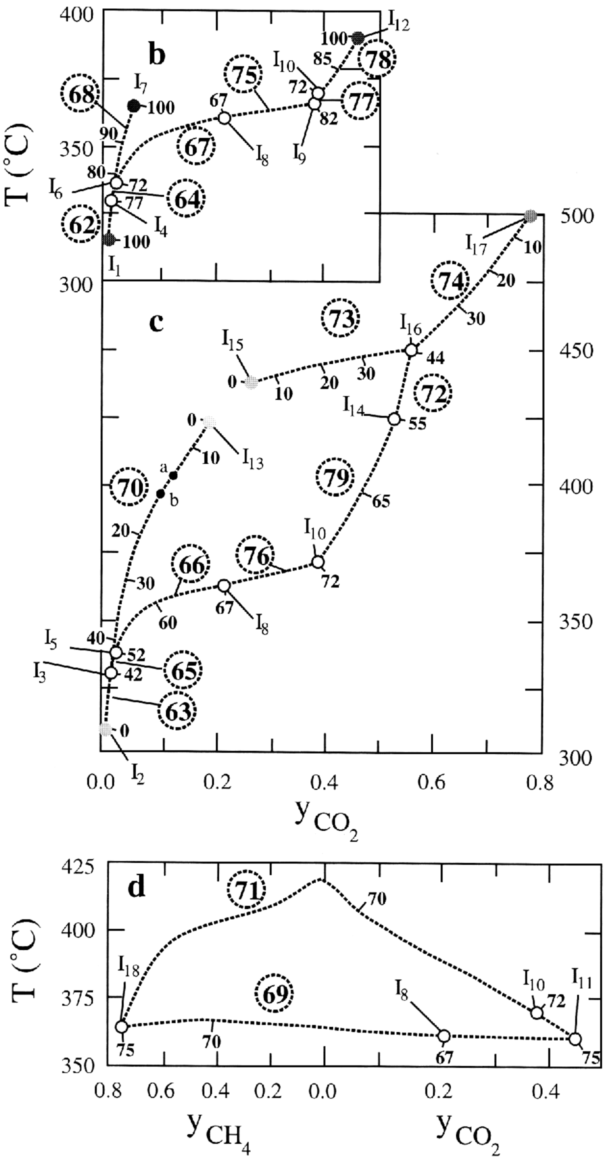

Fig. 10b-d. Composition of chlorite (molar Mg/(Mg + Fe) × 100%) in CFMASH reactions shown in Fig. 10a.

compositions are listed in Table 9 and the stability ranges of univariant reactions are listed in Table 10.

Divariant reactions in CFMASH

The T-X(Fe) diagrams in Fig. 11 illustrate the effects of Fe-Mg solid solution on the stabilities of sudoite, chlorite, dolomite and chloritoid. These diagrams were constructed assuming a saturation hierarchy of SiO_2-Al_2O_3-CaO. Thus, at $y_{CO_2} = 0.0$, the stable low-temperature assemblage is Chl + Kln + Cal + Qtz + Gr + fluid. The last four solids are the buffering phases. The buffering phases change as temperature increases. This is denoted by dashed lines in Fig. 11. In fluids with $y_{CO_2} = 0.0$, there is little difference between the FMASH and CFMASH system, except for the addition of the Ca-bearing phases calcite and margarite. In Mg-rich rocks, sudoite forms from the divariant reaction Kln + Chl = Sud or Prl + Chl = Sud in more intermediate Mg compositions. Chloritoid will form by similar reactions in Fe-rich rocks. However, Frey (1987a) suggests that chloritoid only rarely coexists with kaolinite. This implies that either reactants and products are never found together, bulk rock compositions are rarely Fe-rich enough, or that this reaction is kinetically inhibited.

At higher y_{CO_2} values, dolomite is stable as opposed to chlorite. This changes the sudoite and chloritoid forming reactions to those involving dolomite. The effect of increasing y_{CO_2} is to form sudoite and chloritoid at higher temperatures. The divariant reaction most commonly cited for formation of chloritoid, Prl + Chl = Cld + Qtz + H_2O (Frey & Wieland, 1975; Frey, 1987b), is stable in H_2O-rich fluid regions and carbonate-free rocks. At higher y_{CO_2} values and in carbonate-bearing rocks, it is metastable in the CFMASH system with respect to reactions involving dolomite, [66] and [70], Table 8d. In the presence of carbonate, chloritoid-forming divariant reactions are Dol + Prl = Cal + Cld + Qtz + CO_2 [41], Dol + Prl = Ma + Cld + Qtz + H_2O + CO_2 [42], and Ma + Dol + H_2O = Cal + Cld

Table 9a. CFMASH invariant points at 2 kbar.

Invariant Point	Assemblage (Mg/(Mg + Fe) × 100 %)
I_1	Dol(100) Cal Chl(100) Kln Sud(100)
I_2	Dol(0) Cal Chl(0) Kln Cld(0)
I_3	Dol(32) Cal Chl(34) Kln Ma Cld(8)
I_4	Dol(82) Cal Chl(80) Kln Ma Sud(98)
I_5	Dol(58) Prl Chl(52) Kln Ma Cld(16)
I_6	Dol(72) Prl Chl(72) Kln Ma Sud(97)
I_7	Dol Cal Chl(100) Ma Sud(100)
I_8	Prl Chl(70) And Cld(33) Sud(97)
I_9	Dol(72) Prl Chl(72) And Ma Cld(41)
I_{10}	Dol(82) Prl Chl(80) And Ma Sud(98)
I_{11}	Dol(100) Chl(100) And Ma Sud(100)
I_{12}	Dol(0) Cal Chl(0) Ma Cld(0)
I_{13}	Dol(0) An Chl(0) Ma Cld(0)
I_{14}	Dol(32) And Chl(39) Ma An Cld(16)
I_{15}	Dol(0) Chl(0) And An Cld(0)
I_{16}	Prl Chl(72) And Ma Cld(33) Sud(97)

Table 9b. CFMASH invariant points at 3 kbar.

Invariant Point	Assemblage (Mg/(Mg + Fe) × 100 %)
I_1	Dol(100) Cal Chl(100) Kln Sud(100)
I_2	Dol(0) Cal Chl(0) Kln Cld(0)
I_3	Dol(42) Cal Chl(42) Kln Ma Cld(16)
I_4	Dol(72) Cal Chl(77) Kln Ma Sud(98)
I_5	Dol(58) Prl Chl(52) Kln Ma Cld(16)
I_6	Dol(72) Prl Chl(72) Kln Ma Sud(97)
I_7	Dol(100) Cal Chl(100) Ma Sud(100)
I_8	Dol(62) Prl Chl(67) Ma Cld(33) Sud(97)
I_9	Dol(72) Prl Chl(82) Ky Sud(98)
I_{10}	Dol(72) Chl(72) Ky Ma Cld(41) Sud(98)
I_{11}	Dol(72) Prl Chl(75) Ky Cld(41) Sud(98)
I_{12}	Dol(100) Chl(100) Ky Ma Sud(100)
I_{13}	Dol(0) Cal Chl(0) Ma Cld(0)
I_{14}	Dol(52) Ky Chl(55) And Ma Cld(24)
I_{15}	Dol(0) An Chl(0) Ma Cld(0)
I_{16}	Dol(42) And Chl(44) Ma An Cld(16)
I_{17}	Dol(0) Chl(0) And An Cld(0)
I_{18}	Prl Chl(75) Ky Ma Cld(41) Sud(98)

Table 10. Diagnostic assemblages in CFMASH at 3 kbar.

Univariant Reaction #	Limiting IP's	Assemblage (+ Qtz, Gr, fluid) Dol	Chl	Sud	Cld	other	Stability Range T (°C)	y_{CO_2}
[62]	1 - 4	100 - 72	100 - 77	100 - 98		Kln, Ma, Cal	310 - 330	0,01
[63]	2 - 3	42 - 0	42 - 0		16 - 0	Kln, Cal	320 - 330	0,01
[64]	4 - 6	72	82 - 77	98		Kln, Ma	330 - 340	0,01 - 0,04
[65]	3 - 5	58 - 42	52 - 42		16	Kln, Ma	330 - 340	0,01 - 0,04
[66]	5 - 8	72 - 58	82 - 52		33 - 16	Prl, Ma	340 - 360	0,04 - 0,33
[67]	6 - 8	72 - 62	72 - 67	97		Prl, Ma	340 - 360	0,04 - 0,33
[68]	6 - 7	100 - 72	100 - 72	100 - 97		Ma, Cal	340 - 370	0,04 - 0,08
[69]	11 - 18		75 - 67	98	41 - 33	Prl	360	-0,74*-0,56
[70]	3 - 13	42 - 0	42 - 0		16 - 0	Ma, Cal	330 - 420	0,01 - 0,26
[71]	11 - 18		75 - 70	98	41 - 33	Ky	360 - 370	-0,74*-0,56
[72]	14 - 16	52 - 42	55 - 44		24 - 16	And, An	430 - 450	0,63 - 0,66
[73]	15 - 16	42 - 0	44 - 0		16 - 0	Ma, An	440 - 450	0,35 - 0,66
[74]	16 - 17	42 - 0	44 - 0		16 - 0	And, Ma	450 - 500	0,66 - 0,85
[75]	8 - 9	72 - 62		98 - 97	41 - 33	Prl, Ma	360 - 370	0,33 - 0,47
[76]	8 - 10	72 - 62	72 - 67	98 - 97	41 - 33	Ma	360 - 370	0,33 - 0,48
[77]	9 - 10	72		98	41	Ky, Ma	370	0,47 - 0,48
[78]	10 - 12	100 - 72	100 - 72	100 - 98		Ky, Ma	370 - 390	0,48 - 0,56
[79]	10 - 14	72 - 52	72 - 55		41 - 24	Ky, Ma	370 - 430	0,48 - 0,63

+ CO_2 [45]. The first two represent low-temperature formation of chloritoid.

Additions of Fe to sudoite, chlorite, and dolomite collapse the CMASH field bounded by the divariant reactions [22], [23], [29], [31], and [26] (in Fig. 6) onto the univariant reaction [67] (Fig. 10a). Thus, the CMASH system represents the maximum range of stability for sudoite. Changes in the activity of the sudoite component greatly restrict the stability field of sudoite. The maximum Fe content of sudoite in Fig. 10a is at invariant points I_6, and I_8 (sud = 97%, cch = 70). This is more Mg-rich than sudoite found in the Liassic (sud = 74). This is probably due to inaccurate estimates for Fe-sudoite thermodynamic data. In the CFMASH system, the upper stability limit of the assemblage Prl + Dol + Sud is marked by [2], [62], [64], and [67], and the lower limit is set by reaction [22] for CMASH. This defines the stability range of the assemblage Prl + Dol + Sud to 300 to 340°C at 2 kbar. This suggests that these minerals may constitute a good index assemblage and geothermometer.

Margarite is a product of CASH reaction [5] and many of the univariant ([63] through [68] and [76]) and divariant reactions ([28], [31], [42], and [46]) that consume dolomite. If calcite is abundant, pyrophyllite will be consumed in [5] which may occur before the formation of chloritoid. This would cause the formation of chloritoid to proceed *via* reactions consuming margarite such as [70] or [45].

Reactions in the Liassic

Based on assemblages observed in this study and by Frey (1970 and 1978), inferred reactions in the Liassic progress as follows. The lowest variance low-temperature assemblage is Kln + Chl + Dol + Cal (+ Qtz + Gr + fluid). The pyrophyllite isograd occurs by [3] approximately at the diagenetic-anchizone transition. In the Liassic shales, sudoite is found with chlorite, pyrophyllite, quartz, with and without calcite and dolomite. The formation of sudoite occurs in dolomite-bearing, Mg-rich, aluminous rocks in the anchizone by Dol + Prl + H_2O = Cal + Sud + Qtz + CO_2 [24a] (between CMASH invariant points I_{S1} and I_{S2} in Fig. 6) or by reaction of kaolinite in [24]. If the rock is carbonate-free, sudoite may form by Kln + Chl + H_2O = Sud + Qtz in more Mg-rich rocks or Prl + Chl + H_2O = Sud + Qtz in intermediate composition rocks. Though data on sudoite occurrences in the Liassic are limited, owing to the difficulty of detecting it by powder X-ray diffraction in the presence of trioctahedral chlorite, sudoite has not been observed to coexist with margarite. Therefore, it is assumed that sudoite is consumed by univariant reactions [63], [66], and [67] or divariant reaction [31].

In Fe-rich aluminous rocks, chloritoid forms by a similar paragenesis as sudoite. In fluids with nearly X_O = 1/3, chloritoid would form from Prl + Chl = Cld + Qtz + H_2O (possibly Kln + Chl = Cld + Qtz + H_2O if the Fe-content of the rock is very high). In carbonate-bearing rocks at higher y_{CO_2}, the univariant reaction [66] or divariant reactions [41] and [42] produce chloritoid. Chloritoid-consuming reactions in dolomite-bearing rocks are the divariant reactions [44] and [49]. Additions of Mg to chloritoid shrink its stability field relative to pure chloritoid. Additional chloritoid may form by univariant reaction [70] if margarite is present, and at higher temperatures by [73] if calcite has not consumed margarite to form anorthite. Above these reactions, chloritoid is consumed by divariant reactions [43], [44], and [55].

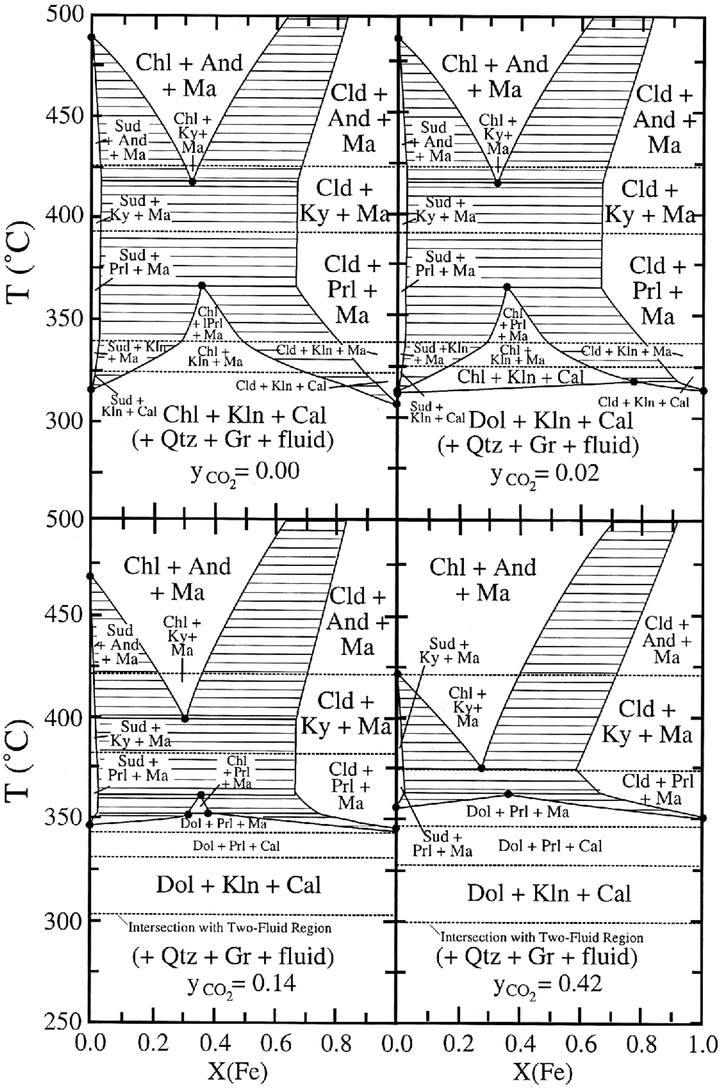

Fig. 11. Plot of temperature verses composition of Fe-Mg minerals in the system CFMASH with quartz, graphite, a Ca-bearing phase (calcite or margarite), and an aluminosilicate phase present for various fluid compositions. Horizontal dashed lines are temperatures for reactions changing the buffering phases.

The important feature common to reactions that form index minerals sudoite, chloritoid, and margarite is that, for fluid compositions where $X_O > 1/3$, they are predominantly decarbonation reactions. These reactions are different from those commonly proposed. The importance of reactions between carbonate and silicate minerals at low metamorphic temperatures has been under emphasized in the literature (for some exceptions see Zen, 1959, and Muffler & White, 1969). The utility of carbonate–silicate equilibria is that they may yield metamorphic temperatures as well as information on fluid compositions and fluxes.

Comparisons of predicted stability fields and geothermometry in the Liassic

Table 11 lists for selected samples their mineralogy, estimated metamorphic temperatures from phase equilibria, calcite-dolomite thermometry, and chloritoid-chlorite thermometry and estimates of compositions of coexisting fluids. One sample from the anchizone (MF-647) from Guggenegg contains a low-variance assemblage that includes sudoite. Temperature estimates from phase equilibria and calcite-dolomite geothermometry for this sample are in good agreement at approximately 310–350°C. The stability field of sample MF-647 is defined by the divariant reaction Dol + Prl = Sud [24a] (with reduced activities of dol and sud) and bounded by CASH reactions Kln = Prl [3] and Cal + Prl = Ma [5]. With the absence of sudoite in sample MF-650, the less diagnostic assemblage indicates an upper temperature limit of 330°C. However, calcite-dolomite temperatures are much higher for sample MF-650 (380–400°C).

Samples from Gravera contain chlorite and chloritoid, and in some cases calcite and dolomite. Chloritoid-chlorite and calcite-dolomite temperatures for Gravera are both

Table 11. Estimated stability fields for Liassic shales.

Rock	Loc.*	Assemblage†	Reactions	kbar	T °C (PE)‡	T °C (C-D)§	T °C (C-C)‖	y_{CO_2}	Grade
MF-647	Gg	Sud-Cal-Dol-Prl-Chl	3, 24a, 5	2	330	310-350	–	0.21-0.25	anchizone
MF-650	Gg	Cal-Dol-Prl-Chl	2, 3, 5, 23	2	≤330	380-410	–	≥0.15	anchizone
MF-551	Kp	Cal-Dol-Chl	–	2	–	320-400	–	–	anchizone
MF-736	Pp	Cal-Dol-Chl	–	3	–	410-430	–	–	epizone
MF-928	Gv	Cal-Dol-Cld-Chl	3, 41, 44, 45	3	330-340	220-360	380-420	0.02	epizone
MF-897	VG	Ma-Cld-Chl	–	3	–	–	450-540	–	epizone
MF-900	VG	Cal-Dol-Ma-Chl	10, 48, 49	3	370-450	450-470	–	0.05-0.45	epizone
MF-899	VG	Cal-Dol-Ma-Cld-Chl	70	3	340-370	480-510	680-990	0.02-0.06	epizone
MF-857	AT	Ma-Cld-Chl	–	3	–	–	340-650	–	epizone
DrT 1210	Sd	Cal-Dol-Cld-Chl	3, 41, 44, 45	3	330-350	440-460	410-460	0.02-0.04	epizone

Note: * = location, Gg = Guggenegg, Kp = Klausenpass, Pp = Panixerpass, Gv = Gravera, VG = Val Gierm, AT = Alp Tgom, Sd = Sedrun; † = + Qtz + Gr + muscovite + pyrite ± paragonite; ‡ = temperature recorded by phase equilibria; § = calcite-dolomite temperature; ‖ = chloritoid-chlorite temperature of VGBP.

lower than other epizone samples (Table 11). If it is assumed that pyrophyllite was a reactant, phase equilibria predict temperatures of 330–340°C which is consistent with the VGBP chloritoid-chlorite calibration. The only reaction that can form chloritoid at 250°C (predicted by SP and HP) is [39] at high values of y_{CO_2}. It is difficult to reconcile such low temperatures with estimates from other samples from the Urseren Zone and the fact that illite crystallinity measurements indicate conditions of the epizone. Therefore, the SP and HP geothermometry for Gravera samples are not prefered.

Sample MF-899 from Val Gierm contains a low-variance assemblage defined by [70]. The temperature of stability for this sample predicted from phase equilibria (340–370°C) is much lower than those predicted by calcite-dolomite (480–510°C) and chloritoid-chlorite geothermometry (680–990°C). However, the chloritoid-chlorite temperature in sample MF-897 (450–540°C) from the same area is more consistent with phase equilibria. Sample DrT 1210 near Sedrun has the same assemblage as at Gravera, yet geothermometry predicts higher temperatures in Sedrun.

Phase equilibria generally predict lower temperatures than geothermometry in the anchizone and epizone. The most likely source of the discrepancy is the lack of pervasive equilibration in the anchizone, and, errors in the thermodynamic database, in particular, the thermodynamic parameters for margarite, chloritoid, and magnesiochloritoid.

Estimation of fluid compositions

The diagenetic-grade assemblage is Kln + Chl + Dol + Cal (+ Qtz + Gr + fluid). This assemblage constrains equilibrium fluids to being close to $X_O = 1/3$ (see reactions [21] in CMASH and [38] in CFASH). This is interesting in that the calculation of the fluid miscibility gap predicts two fluids at low temperatures one of which is very H_2O-rich. Mullis *et al.* (1994) found that fluid inclusions in the diagenetic zone were dominated by higher hydrocarbon fluids up to 200°C and by CH_4 to about 270°C. Though CH_4-rich fluids are compatible with the above assemblage, H_2O-rich fluid inclusions should also be found. Mullis *et al.* (1994) did not report any H_2O-rich inclusions in the methane zone. To complicate the issue, the pyrophyllite isograd occurs by reaction [3] at approximately the diagenetic-anchizone. Mullis *et al.* (1993) placed this boundary at 230 ± 10°C. This would dictate that fluid compositions be extremely CO_2 or CH_4-rich. If fluid compositions were closer to $X_O = 1/3$, then the pyrophyllite isograd would be closer to 330°C, which is unreasonably high. To reconcile these discrepancies, either the fluid must not be in equilibrium with the mineral assemblage, or the fluid trapped by the inclusions do not represent the peak metamorphic fluid reacting with the rock.

In the anchizone, sample MF-647 indicates y_{CO_2} values of 0.21 to 0.25 (Table 11). Correlations between illite crystallinity and vitrinite reflectance data for Liassic samples in the Glarus Alps, along with fluid composition zones from other localities in the Helvetic zone, indicate that Guggenegg and Klausenpass are in the H_2O–rich zone of the upper anchizone which is above 270°C (Frey *et al.*, 1980b). Thus, the phase equilibria and fluid inclusions are in agreement in the high anchizone.

Margarite is stable at values of $X_O > 1/3$. Epizone samples containing margarite record more H_2O-rich fluids than in the anchizone. For example, the assemblage Cal + Dol + Cld + Ma + Chl + Qtz, which is correspond to [70], records $y_{CO_2} = 0.02–0.18$. Mullis *et al.* (1994) also found H_2O-rich fluid inclusions in the epizone. At higher grades, Mullis *et al.* (1994) observed more CO_2-rich inclusions. Frey (1978) described Liassic marly phyllites and schists from Valle Cavalasca and Lukmanierpass that contain the assemblage Ma + Cz + An (andesine) + paragonite + Chl + Cal + Dol + Qtz. This assemblage is invariant in CASH and is located at $y_{CO_2} = 0.17$ (without corrections for reduced ma and an activities and at 430°C and 3 kbar). Higher pressures would shift equilibrium to higher y_{CO_2} values and temperatures. Thus, the formation of Cz and plagioclase is consistent with more CO_2-rich fluids at higher grades.

Calculation of reaction progress and fluid fluxes

Metamorphism, traditionally thought of as a thermal process, can also result from chemical interactions between

Table 12. Mineral compositions and modal abundances.

MF-647	Mu	Prl	Pa	Chl	Sud	Cal	Dol	Qtz	wr
vol (cm^3)	30.7	18.1	3.8	4.6	4.2	485.7	1.1	441.8	
n (mol/l)	0.218	0.141	0.029	0.022	0.021	13.198	0.017	19.471	33.12
Na (mol/l)	0.064	0.016	0.478	0.008	0.006	0.000	0.000	0.000	0.030
K (mol/l)	0.866	0.029	0.181	0.002	0.010	0.000	0.000	0.000	0.199
Ca (mol/l)	0.006	0.008	0.011	0.026	0.033	0.973	1.168	0.000	12.872
Si (mol/l)	3.115	3.871	3.169	2.537	3.114	0.000	0.000	1.000	20.910
Al (mol/l)	2.716	2.095	2.835	3.086	3.913	0.000	0.000	0.000	1.120
Mg+Fe (mol/l)	0.167	0.083	0.067	4.385	1.861	0.025	0.826	0.000	0.528
molar volume	140.8	128.1	132.1	212.4	203.0	36.8	64.5	22.7	990.1

DrT 1210	Mu	Chl	Cld	Cal	Dol	Qtz	wr
vol	271.8	39.1	29.1	178.5	79.9	375.9	
n	1.930	0.184	0.418	4.839	1.231	16.567	25.17
K	0.734	0.025	0.035	0.000	0.000	0.000	1.4356
Ca	0.074	0.090	0.016	0.941	1.100	0.000	6.0725
Si	3.016	2.663	1.035	0.000	0.000	1.000	23.31
Al	2.906	2.976	1.970	0.000	0.000	0.000	6.9799
Mg+Fe	0.093	4.091	0.927	0.059	0.990	0.000	2.8241
molar volume	140.8	212.4	69.7	36.9	64.9	22.7	974.3

MF-852	Mu	Pa	Ma	Chl	Qtz	wr
vol	130	50	50	10	760	
n	0.923	0.379	0.386	0.047	33.495	35.23
K+Na	0.943	0.844	0.095	0.012	0.000	1.2273
Ca	0.002	0.116	0.895	0.002	0.000	0.3911
Si	3.057	2.826	2.052	2.585	1.000	38.301
Al	2.880	3.200	3.946	3.013	0.000	5.5348
Fe+Mg+Mn	0.081	0.010	0.028	4.287	0.000	0.2914
molar volume	140.8	132.0	129.6	212.2	22.7	1000

MF-857	Mu	Pa	Ma	Chl	Cld	Qtz	wr
vol	450	100	50	10	150	240	
n	3.195	0.758	0.386	0.047	2.170	10.577	17.13
Ca	0.002	0.116	0.895	0.002	0.002	0.000	0.444
Si+Al	5.937	6.000	5.998	5.598	3.007	1.000	43.198
Fe+Mg+Mn	0.081	0.010	0.028	4.287	0.967	0.000	2.5781
molar volume	140.8	132.0	129.6	212.2	69.1	22.7	1000

MF-537 (protolith to MF-857)	Mu	Pa	Prl	Chl	Dol	Qtz
Ca	0.002	0.116	0.000	0.011	0.990	0.000
Si+Al	5.937	6.000	6.000	5.801	0.000	1.000
Fe+Mg+Mn	0.081	0.010	0.000	3.824	1.010	0.000
molar volume	140.8	132.0	128.1	212.2	36.9	22.7

rocks and reactive fluids (Ferry, 1988; Valley, 1986). The evidence for fluid infiltration comes from extensively homogenized oxygen isotope ratios (Valley, 1986) and the calculation of volumes of fluid involved in metamorphism that are greater than the rock porosity (Ferry, 1988). If the fluid is not in equilibrium with the rock, then infiltration produces sharp reaction fronts that propagate along the flow path. No front is produced if local equilibrium is everywhere maintained during flow. Reaction may still take place in this case if there is a temperature and/or pressure gradient along the flow path. Reaction progress in an assemblage that includes reactants and products of the mineral-fluid reaction is a quantitative measure of the time-integrated fluid flux during flow and reaction.

The Liassic marls and slates present an opportunity to determine fluid fluxes at low metamorphic grades because they contain minerals that were produced by decarbonation reactions. Unfortunately, data of this study are inadequate to completely rule out sharp reaction fronts, and hence, to discriminate with certainty between equilibrium and disequilibrium flow. However, since reactants and products do occur together in some samples, it is assumed that observed reactions were driven by fluid flow along temperature and pressure gradients during metamorphism.

Calculations of reaction progress and fluid fluxes followed procedures outlined by Ferry (1984) and Baumgartner & Ferry (1991). Modal abundances of minerals were obtained either from point counting using the electron microprobe or from X-ray maps analyzed with the remote sensing program MULTISPEC. For each sample considered with the latter technique, modes were computed from mass balance relations involving mineral and whole-rock compositions (Ferry, 1984). Molar volumes of minerals were taken from HP93. Model protolith assemblages and mineral compositions were chosen, and the protolith modal abundances were calculated from the

Table 13. Model reactions.

Sample	Reaction (mol per liter rock)
MF-647	0,076 Prl + 0,163 Dol + 0,099 H_2O = 0,002 Mu + 0,002 Pa + 0,022 Chl + 0,195 Cal + 0,163 Qtz + 0,021 Sud + 0,131 CO_2
MF-852	0,369 Prl + 1,001 Pa + 0,016 Chl + 0,231 Cal = 0,857 Mu + 0,934 Qtz + 0,386 Ma+ 0,192 H_2O + 0,231 CO_2
MF-857	5,145 Prl + 0,510 Chl + 0,422 Dol = 2,170 Cld + 0,386 Ma+ 1,481 Qtz + 4,629 H_2O + 0,442 CO_2
DrT 1210	0,244 Ma+ 0,612 Dol + 0,064 Qtz + 0,345 H_2O = 0,007 Mu + 0,041 Chl + 0,936 Cal + 0,418 Cld + 0,288 CO_2

whole-rock composition. The reaction driven by fluid infiltration is the difference between protolith and present molar abundances of minerals. Abundances, mineral compositions, and reactions are listed in Tables 12 and 13.

Calculations of time-integrated fluid flux were based on the model of Baumgartner & Ferry (1991), which relates the progress of dehydration-decarbonation reactions, the composition of the evolving fluid, the temperature- and pressure-dependence of fluid composition, the temperature and pressure gradients along the flow path:

$$q_t = \frac{\overline{V}_{fl}\left(n_{CO_2} - y_{CO_2}(n_{CO_2} + n_{H_2O})\right)}{\left[\left(y_{CO_2}/_T\right)_P\left(T/_z\right) + \left(y_{CO_2}/_P\right)_T\left(P/_z\right)\right]} \qquad (1)$$

where q_t is the time-integrated volume fluid flux, $\overline{V}_{fl}$ is the molar volume of the fluid, and n_{CO_2} and n_{H_2O} are the number of moles of the volatile species produced (+) or consumed (–) by a reaction per volume of rock. The parameter y_{CO_2} is the mole fraction of CO_2 in the fluid, $(\partial y_{CO_2}/\partial P)_T$ and $(\partial y_{CO_2}/\partial T)_P$ are the inverse of the slopes of equilibria on P–y and T–y diagrams, and $\partial P/\partial z$ and $\partial T/\partial z$ are the pressure and temperature gradients along the path of the fluid. To use this equation, the direction of the fluid flow needs to be constrained. This may be accomplished by examining the signs and magnitudes of the variables in equation 1. Illite "crystallinity" data of Frey (1970) and Frey & Wieland (1975) show that Liassic samples increase in grade (temperature) to the south. The parameter $(\partial y_{CO_2}/\partial P)_T\partial P/\partial z$ is small compared to $(\partial y_{CO_2}/\partial T)_P\partial T/\partial z$ and is therefore ignored as a simplification. The phase equilibria show that the production of margarite, chloritoid, and sudoite mainly involves decarbonation reactions (Table 13). For reactions considered here ([5], [24a], [66], and [70]), $(\partial y_{CO_2}/\partial T)_P$ is positive and q_t is defined as positive along the path of the flow. For most combinations of n_{CO_2} and n_{H_2O} in decarbonation reactions, the numerator in Equation 1 is positive. Therefore, $\partial T/\partial z$ was also positive and flow was up-temperature.

Parameters used in calculating fluxes are listed in Table 14. The value of $\partial T/\partial z = 3.3 \times 10^{-5}$°/cm was estimated from the difference in metamorphic temperature between the Glarus Alps and the Urseren Zone. Based on assessments of Ferry & Dipple (1991) and Léger & Ferry (1993), flux calculations are probably accurate to within an order of magnitude. This uncertainty is a minimum for the Liassic samples, whose fine grain size impedes calculation of modal abundances, and whose heterogeneous mineral compositions generate additional uncertainties.

Four samples were used in the flux calculations – one from the anchizone and three from the epizone. A flux for sample MF-647 from Guggenegg can be calculated for the formation of sudoite from dolomite and pyrophyllite. The model reaction is [24a], and the estimated whole-rock reaction is given in Table 13. Temperatures and fluid compositions were limited by the intersection of [3], [5], and [24a] with reduced mineral activities. This gives a narrow stability field for sample MF-647. The volatiles given off by the reaction are pure CO_2, and some H_2O is consumed. The flux calculated for MF-647 is between 5×10^3 and 8×10^3 cm.

Table 14. Fluid flux calculation parameters.

Sample	MF-647		MF-852		MF-857		DrT 1210	
Grade	Anchizone		Epizone		Epizone		Epizone	
	q_t (min)	q_t (max)	q_t (min)	q_t (max)	q_t (min)	q_t (max)	q_t (min)	q_t (max)
T (°C)	328	330	350	336	355	336	350	331
Reaction #	24a	24a	5	5	66	66	70	70
P (bars)	2000	2000	3000	3000	3000	3000	3000	3000
y_{CO_2}	0,213	0,253	0,50	0,045	0,07	0,045	0,035	0,024
$\partial y/\partial T$ (°C^{-1})	$2{,}0 \times 10^{-2}$	$1{,}4 \times 10^{-2}$	∞	$2{,}3 \times 10^{-3}$	1×10^{-2}	$2{,}3 \times 10^{-3}$	$7{,}5 \times 10^{-4}$	$6{,}8 \times 10^{-4}$
Vfl (cm^3)	28,5	29,9	21,3	21,3	22,4	21,3	21,2	20,6
n_{CO_2} (mol/l)	0,131	0,131	0,231	0,231	0,423	0,423	0,288	0,288
$\sum n_j$ (mol/l)	0,032	0,032	0,423	0,423	6,29	6,29	-0,058	-0,058
q_t (cm^3/cm^2)	5×10^3	8×10^3	0	6×10^4	0	4×10^4	$2{,}5 \times 10^5$	$2{,}7 \times 10^5$

The time-integrated fluxes calculated for the samples from the epizone represent the minimum and maximum fluxes needed to completely consume one of the reactants. The range in calculated fluxes is a function of the range of possible temperatures for a particular reaction. Fluids can continue to infiltrate the rocks after one of the reactants has been exhausted, but flow will not be recorded by the mineral modal abundances. Therefore, time-integrated fluxes reported for the epizone are minimum estimates. The model reaction for sample MF-852 from Alp Tgom is [5]. The time-integrated flux is zero if the reaction occurred at the temperature maximum for reaction [5] where y_{CO2} = 0.5 and $(\partial y_{CO_2}/\partial T)_P = {}^\circ$. The maximum time-integrated flux (6 × 10^4 cm^3/cm^2) occurs if the reaction proceeded at the invariant point at the intersection of [5] and [3], where $(\partial y_{CO_2}/\partial T)_P$ is 2.3 × 10^4 (deg^{-1}) (Fig. 11a). The model reaction for sample MF-857 is [66], and the protolith contained pyrophyllite and dolomite that were consumed during formation of chloritoid and margarite. The compositions of minerals in the protolith to MF-857 were taken as those in sample MF-537 from Klausenpass in the anchizone. The time-integrated flux is 0 cm^3/cm^2 if reaction occurred at 355°C and a maximum (4 × 10^4 cm^3/cm^2) for reaction at invariant point 19 (Fig. 11a). Reaction in sample DrT 1210 is modeled by [70] which is a hydration-decarbonation reaction. The protolith was assumed to contain margarite that had a composition the same as macrocrystalline margarite in sample LP-9 from Lukmanierpass (Livi *et al.*, 1997). The stability field of this model reaction is limited by the composition of chlorite along [70] in Fig. 11b. The minimum time-integrated flux recorded by DrT 1210 is 2.5–2.7 × 10^5 cm^3/cm^2.

The time-integrated fluxes calculated above can be compared with those from studies of regional metamorphism in New England. Baumgartner & Ferry (1991) calculated fluxes for the biotite-forming reaction muscovite + 3 Dol + 2 Qtz = biotite + 2 Cal + An + 4 CO_2 in carbonate rocks of the Waterville and Vassalboro Formations from Maine at 430°C and y_{CO_2} = 0.05–0.15. Calculated time-integrated fluxes range from 0 to 2 × 10^6 cm^3/cm^2. Léger & Ferry (1993) calculated time-integrated fluxes for several reactions that occur in siliceous carbonate rocks of the Waits River Formation in north-east Vermont. The lowest grade reaction studied was paragonite + Cal + 2 Qtz = albite + An + CO_2 + H_2O at 450°C and y_{CO_2} = 0.03–0.08. The time-integrated fluxes recorded for this reaction range from 2 × 10^3 to 2.4 × 10^4 cm^3/cm^2. The biotite-forming reaction occurs in the Waits River Formation at 490°C and y_{CO_2} = 0.2–0.3. Fluxes recorded for this reaction are between 4.3 × 10^3 to 4.6 × 10^4 cm^3/cm^2, but they are generally closer to 3 × 10^4 cm^3/cm^2.

The time-integrated flux calculated for sample MF-647 is comparable to those calculated by Léger & Ferry (1993) for the plagioclase-forming reaction, even though the peak temperature for sample MF-647 was only 330°C. This is strong evidence for infiltration-driven metamorphism in the Liassic rocks. Time-integrated fluxes seem to be even greater in the epizone as is evident from sample DrT 1210. If this sample is representative of the epizone, then fluxes in the Urseren Zone are on the same order as those calculated for biotite isograds in New England (10^4–10^6 cm^3/cm^2).

Phase equilibria at the boundaries of the anchizone

Frey (1970 and 1978) measured the illite "crystallinity" of the Liassic and Quartenschiefer shales. Illite "crystallinity" values cannot be determined on samples that contain mixed paragonite-muscovite. Because most of the Liassic aluminous shales contain this mixture, grade was estimated by samples from associated Triassic redbeds without paragonite. This study allows determinations of grade by illite "crystallinity" to be compared to determinations based on calculated phase equilibria.

The diagenetic zone is characterized by the CFMASH assemblage Kln + Chl ± Dol ± Cal (+ Qtz + organic matter). In the anchizone, the assemblage is Chl ± Prl ± Sud ± Dol ± Cal. The anchizone transition correlates with the formation of pyrophyllite in the Glarus Alps and is estimated to occur at 230°C (Mullis *et al.*, 1993). Unfortunately, the proper samples to evaluate the diagenetic-anchizone transition (coexisting pyrophyllite and kaolinite) are missing in the Liassic sequence. In the Liassic, margarite is found in the epizone and not in the anchizone (Frey, 1978; Livi *et al.*, 1997). Therefore, [5] should place the upper limit on the anchizone at 350°C and 3 kbar. Evidence is presented in Livi *et al.* (1997) that margarite first forms as very small high-Ca domains within paragonite and muscovite. This may indicate that margarite has difficulty nucleating as a separate phase and that formation temperatures may be higher than predicted by our calculations. The anchizone-grade sample MF-647 from Guggenegg records temperatures near 330°C. Thus, based on phase equilibria and calcite-dolomite thermometry, the upper temperature limit for the anchizone in the Glarus Alps should be greater than 330°C and possibly higher than 350°C. Kisch (1987) used an apparent correlation between illite “crystallinity” and the location of the prehnite-pumpellyite facies in basic rocks to define the limits of the anchizone. Experimental phase equilibria, combined with oxygen isotope data, set a lower limit of 200–250°C and an upper limit of 300°C. The discrepancy in the upper limit may be related to kinetic factors affecting both the formation of equilibrium phases and the rate of illite recrystallization which would be unique to each geologic setting.

Summary

Although low-grade metamorphic studies are hindered by their fine-grained nature and potential for disequilibrium, this study shows that it is possible to apply modern metamorphic petrology tools to these rocks if care is taken to assess the degree of equilibration. Mineral compositions, estimated temperatures, and mineral assemblages indicate that in the Liassic black shales of central Switzerland approach equilibration, although not perfectly, in the upper anchizone. The petrologic framework for estimating the physical conditions of low-grade metamorphism, especially for fluid-rock interactions, have been presented here. Many more refinements of the petrologic grids will be necessary, and techniques to describe the extent of equilibrium and identification of reacted portions of the rocks will need to be developed. In addition, the identification of sudoite in low-grade assemblages is encouraged as this index mineral has great potential, but is often hidden by more dominant coexisting chlorites. The role of carbonate-silicate reactions have been under emphasized in low-grade metamorphic studies. This study demonstrates the value of investigating such reactions.

Acknowledgments: This article is dedicated to the memory of Martin Frey who died in his beloved Alps in the fall of 2000. His influence in low temperature metamorphism will be felt for many years to come. The authors gratefully acknowledge support from the National Science Foundation through grants EAR-0073955, EAR-0001080, and EAR-9512438, the U.S. Department of Energy (DE-FG02-89ER14074), and grants from the Keck Foundation for partial funding of the Johns Hopkins High Resolution Electron Microbeam Facility.

References

Abart, R., Connolly, J.A.D., Trommsdorff, V. (1992): Singular point analysis: Construction of Shreinemakers projections for systems with a binary solution. *Am. J. Science*, **292**, 778-805.

Albee, A.L. (1972): Metamorphism of pelitic schists: Reaction relations of chloritoid and staurolite. *Geol. Soc. Am. Bull.*, **83**, 3249-3268.

Anovitz, L.M. & Essene, E.J. (1987): Phase equilibria in the system $CaCO_3$-$MgCO_3$-$FeCO_3$. *J. Petrol.*, **28**, 389-414.

Armstrong, J.T. (1989): CITZAF: combined ZAF and phi-rho (Z) electron beam correction programs. California Institute of Technology, Pasadena, Calif.

Ashworth, J.R. & Evirgen, M.M. (1984): Mineral chemistry of regional chloritoid assemblages in the chlorite zone, Lycian Nappes, South-west Turkey. *Min. Mag.*, **48**, 159-165.

Baker, J., Holland, T.J.B., Powell, R. (1994): The effect of Tschermak's substitution on assemblages in aluminous dolomites. *Contrib. Mineral. Petrol.*, **118**, 48-59.

Banfield, J.F., Karabinos, P., Veblen, D.R. (1989): Transmission electron microscopy of chloritoid: Intergrowth with sheet silicates and reactions in metapelites. *Am. Mineral.*, **74**, 549-564.

Baumgartner, L. & Ferry, J.M. (1991): A model for coupled fluid flow and mixed volatile mineral reactions with applications to regional metamorphism. *Contrib. Mineral. Petrol.*, **106**, 273-285.

Berman, R.G. (1988): Internally-consistent thermodynamic data for minerals in the system Na_2O–K_2O–CaO–MgO–FeO–Fe_2O_3–Al_2O_3–SiO_2–TiO_2–H_2O–CO_2. *J. Petrol.*, **29**, 445-522.

Bickle, M.J. & Powell, R. (1977): Calcite-dolomite geothermometry for iron-bearing carbonates: The Glockner area of the Tauern window, Austria. *Contrib. Mineral. Petrol.*, **59**, 281-292.

Biehl, L. & Landgrebe, D.A. (1993): Multispec: Analysis of multispectral image data. Purdue Research Foundation, West Lafayette, Indiana.

Black, P.M. (1975): Mineralogy of New Caledonian Metamorphic Rocks. *Contrib. Mineral. Petrol.*, 269-284.

Buseck, P.R. & Huang, B.-J. (1985): Conversion of carbonaceous material to graphite during metamorphism. *Geochim. Cosmochim. Acta*, **49**, 2003-2016.

Chinner, G.A. (1967): Chloritoid and the isochemical character of Barrow's zones. *J. Petrol.*, **8**, 268-282.

Chopin, C. & Schreyer, W. (1983): Magnesiocarpholite and magnesiochloritoid: Two index minerals of pelitic blueschists and their preliminary phase relations in the model system MgO-Al_2O_3-SiO_2-H_2O. *Am. J. Science*, **283-a**, 72-96.

Connolly, J.A.D. & Cesare, B. (1993): C-O-H-S fluid composition and oxygen fugacity in graphitic metapelites. *J. metamorphic Geol.*, **11**, 379-388.

Connolly, J.A.D. & Kerrick, D.M. (1987): An algorithm and computer program for calculating composition phase diagrams. CALPHAD, **11**, 1-55.

Cruickshank, R.D. & Ghent, E.D. (1978): Chloritoid-bearing rocks of the Horsethief Creek Group, southeasern British Columbia. *Contrib. Mineral. Petrol.*, **65**, 333-339.

Ferry, J.M. (1984): A biotite isograd in south-central Maine, USA: Mineral reactions, fluid transfer, and heat transfer. *J. Petrol.*, **25**, 871-893.

— (1988): Infiltration–driven metamorphism in Northern New England. *J. Petrol.*, **29**, 1121-1159.

Ferry, J.M. & Baumgartner, L. (1987): Thermodynamic models of molecular fluids at the elevated pressures and temperatures of crustal metamorphism. *In* "Thermodynamic Modeling of Geologic Materials: Minerals, Fluids, and Melts", Carmichael, I.S.E. & Eugster, H.P., eds., *Review Mineral.*, **17**, 323-366.

Ferry, J.M. & Dipple, G.M. (1991): Fluid flow, mineral reactions, and metasomatism. *Geology*, **19**, 211-214.

Fox, J.S. (1971): Coexisting chloritoid and staurolite and the staurolite-chlorite isograd from the Agnew Lake area, Ontario, Canada. *Geol. Magazine*, **108**, 205-219.

— (1975): Three-dimensional isograds from the Lukmanier Pass, Switzerland, and their tectonic significance. *Geol. Magazine*, **112**, 547-564.

Frey, M. (1970): The step from diagenesis to metamorphism in pelitic rocks during Alpine orogenesis. *Sedimentology*, **15**, 261-279.

— (1978): Progressive low-grade metamorphism of a black shale formation, Central Swiss Alps, with special reference to pyrophyllite and margarite bearing assemblages. *J. Petrol.*, **19**, 95-135.

— (1987a): The reaction-isograd kaolinite + quartz = pyrophyllite + H_2O, Helvetic Alps, Switzerland. *Schweizer. Mineral. Petrograph. Mitt.*, **67**, 1-11.

— (1987b): Very low-grade metamorphism of clastic sedimentary rocks. *In* "Low-Temperature Metamorphism", M. Frey, ed., Blackie, Glasgow, p 9-58.

Frey, M. & Wieland, B. (1975): Chloritoid in autochthon-parautochthonen sedimenten des Aarmassivs. *Schweizer. Mineral. Petrograph. Mitt.*, **55**, 407-418.

Frey, M., Bucher, K., Frank, E., Mullis, J. (1980a): Alpine metamorphism along the Geotraverse Basel-Chiasso – a review. *Eclogae Geologica Helvetica*, **73**, 527-546.

Frey, M., Teichmüller, M., Teichmüller, R., Mullis, J., Künzi, B., Breitschmid, A., Gruner, U., Schwizer, B. (1980b): Very low-grade metamorphism in external parts of the Central Alps: Illite crystallinity, coal rank and fluid inclusion data. *Eclogae Geologica Helvetica*, **73**, 173-203.

Frey, M., Saunders, J., Schwander, H. (1988): The mineralogy and metamorphic geology of low-grade metasediments, Northern range, Trinidad. *J. Geol. Soc. London.*, **145**, 563-575.

Ghent, E.D., Stout, M.Z., Black, P.M., Brothers, R.N. (1987): Chloritoid-bearing rocks associated with blueschists and eclogites, northern New Caledonia. *J. metamorphic Geol.*, **5**, 239-254.

Giorgetti, G., Goffé, B., Memmi, I., Nieto, F. (1998): Metamorphic evolution of Verrucano metasediments in northern Apennines: New petrological constraints. *Eur. J. Mineral.*, **10**, 1295-1308.

Grambling, J.A. (1983): Reversals in Fe-Mg partitioning between chloritoid and staurolite. *Am. Mineral.*, **68**, 373-388.

Hoefs, J. & Frey, M. (1976): The isotopic composition of carbonaceous matter in a metamorphic profile from the Swiss Alps. *Geochim. Cosmochim. Acta*, **40**, 945-951.

Holland, T.B. (1989): The dependence of entropy on volume for silicate and oxide minerals: a review and a predictive model. *Am. Mineral.*, **74**, 5-13.

Holland, T.B. & Powell, R. (1990): An enlarged and updated internally consistent thermodynamic dataset with uncertainties and correlations: the system K_2O Na_2O-CaO-MgO-MnO-FeO-Fe_2O_3-Al_2O_3-TiO_2-SiO_2-C-H_2-O_2. *J. metamorphic Geol.*, **8**, 89-124.

Karabinos, P. (1981): Deformation and metamorphism of Cambrian and Precambrian rocks on the east limb of the Green Mountains anticlinorium near Jamaica, Vermont. Unpublished Ph.D. Thesis, The Johns Hopkins University.

Kübler, B. (1967): La cristallinité de l'illite et les zones tout à fait supérieures du métamorphisme. *Etages Tectoniques Coll. Neuchatel*, **1967**, 105-122.

Large, D.J., Christy, A.G., Fallick, A.E. (1994): Poorly crystalline carbonaceous matter in high grade metasediments: implications for graphitisation and metamorphic fluid compositions. *Contrib. Mineral. Petrol.*, **116**, 108-116.

La Tour, T., Kerrich, R., Hoder, R., Barnett, R. (1980): Chloritoid stability in very iron-rich altered pillow lavas. *Contrib. Mineral. Petrol.*, **74**, 165-173.

Laird, J. (1988): Chlorites: metamorphic petrology. *In* "Hydrous Phyllosilicates (Exclusive of Micas)", S.W. Bailey, ed, *Review Mineral.*, **19**, 405-447.

Léger, A. & Ferry, J.M. (1993): Fluid infiltration and regional metamorphism of the Waits River Formation, north-east Vermont, USA. *J. metamorphic Geol.*, **11**, 3-29.

Livi, K.J.T., Veblen, D.R., Ferry, J.M., Frey, M. (1997): Evolution of 2:1 layered silicates in low-grade metamorphosed Liassic shales of Central Switzerland. *J. metamorphic Geol.* **15**, 323-344.

Merriman, R.J. & Peacor, D.R. (1999): Very low-grade metapelites: Mineralogy, microfabrics and measuring reaction progress. *In* "Low Temperature Metamorphism," M. Frey & D. Robinson, eds., Blackwell Science Ltd, Oxford, 328.

Mposkos, E. & Perdikatzis, A. (1981): Die paragonit-chloritoid führenden schiefer des südwestlichen Bereiches des Kerkis auf Samos (Griechenland). *N. Jb. Miner. Abh.* **142**, 292-308.

Muffler, L.P.J. & White, D.E. (1969): Active metamorphism of Upper Cenozoic sediments in the Salton Sea geothermal field and Salton trough, southeastern California. *Geol. Soc. Am. Bull.*, **80**, 157-182.

Mullis, J. (1979): The system methane-water as a geologic thermometer and barometer from the external part of the Central Alps. *Bull. Minéral.*, **102**, 526-536.

— (1987): Fluid inclusion studies during very low-grade metamorphism. *In* "Low-Temperature Metamorphism", M. Frey, ed., Blackie, Glasgow, 162-199.

Mullis, J., Stern, W.B., de Capitani, C., Frey, M., Rahn, M., Schwer, P., Wang, H. (1993): Correlation of fluid inclusion temperatures with illite, smectite and chlorite "crystallinity" data and smear slide chemistry in sedimentary rocks from the external parts of the Central Alps (Switzerland). IGCP Project 294, Low Temperature Metamorphism, Symposium, November, 1993, Santiago de Chile.

Mullis, J., Dubessy, J., Poty, B., O'Neil, J. (1994): Fluid regimes during late stages of a continental collision: Physical, chemical, and stable isotope measurements of fluid inclusions in fissure quartz from a geotraverse through the Central Alps, Switzerland. *Geochim. Cosmochim. Acta*, **58**, 2239-2267.

Paradis, S., Velde, B., Nicot, E. (1983): Chloritoid-pyrophyllite-rectorite facies rocks from Brittany, France. *Contrib. Mineral. Petrol.*, **83**, 342-347.

Peacor, D.R. (1992): Diagenesis and low-grade metamorphism of shales and slates. *In* "Minerals and Reactions at the Atomic Scale: Transmission Electron Microscopy", P.R. Buseck, ed. *Review Mineral.*, **27**, 335-380.

Phillips, G.N. (1988): Widespread fluid infiltration during metamorphism of the Witwatersrand goldfields: Generation of chloritoid and pyrophyllite. *J. metamorphic Geol.*, **6**, 311-332.

Ranson, W.A. (2000): Margarite-corundum phyllites from the Appalachian orogen of South Carolina: mineralogy and metamorphic history. *Am. Mineral.*, **85**, 1617-1624.

Rochette, P. (1987): Metamorphic control of the magnetic mineralogy of black shales in the Swiss Alps: toward the use of "magnetic isograds". *Earth Planet. Sci. Letters*, **84**, 446-456.

Sharp, Z., Frey, M., Livi, K.J.T. (1995): Stable isotope variations (H,C,O) in a prograde metamorphic Triassic red bed formation, Central Swiss Alps. *Schweizer. Mineral. Petrograph. Mitt.*, **75**, 147-161.

Shreinemakers, F.A.H. (1924): Singular equilibria. *Versl. Koninklijke Akad. Wetenscap*, **27**, 800-808.

Spear, F. & Cheney, J. (1989): A petrogenetic grid for pelitic schists in the system SiO_2-Al_2O_3-FeO-MgO-K_2O-H_2O. *Contrib. Mineral. Petrol.*, **101**, 149-164.

Theye, T., Seidel, E., Vidal, O. (1992): Carpholite, sudoite, chloritoid in low-grade high-pressure metapelites from Crete and the Peloponnese, Greece. *Eur. J. Mineral.*, **4**, 487-507.

Trümpy, R. (1960): Palaeotectonic evolution of the Central and Western Alps. *Geol. Soc. Am. Bull.*, **71**, 843-908.

Valley, J.W. (1986): Stable isotope geochemistry of metamorphic rocks. *In* "Stable Isotopes in High Temperature Geological Processes", J.W. Valley, H.P. Taylor, J.R. O'Neil, eds., *Review Mineral.*, **16**, 445-490.

Vidal, O., Goffé, B., Theye, T. (1992): Experimental study of the stability of sudoite and magnesiocarpholite and calculation of a new petrogenetic grid for the system FeO-MgO-Al_2O_3-SiO_2-H_2O. *J. metamorphic Geol.*, **10**, 603-614.

Vidal, O., Goffé, B., Bousquet, R., Parra, T. (1999): Calibration and testing of empirical chloritoid-chlorite Mg-Fe exchange thermometer and thermodynamic data for daphnite. *J. metamorphic Geol.* **17**, 25-39.

Wang, P. & Spear, F.S. (1990): A field and theoretical analysis of garnet + chloritoid + biotite assemblages from the Tri-state (MA, CT, NY) Area, USA. *Contrib. Mineral. Petrol.*, **106**, 217-235.

Zen, E.-a. (1959): Clay mineral-carbonate relations in sedimentary rocks. *Am. J. Science*, **257**, 29-43.

Received 7 December 2000
Modified version received 18 November 2001
Accepted 22 January 2002